

1 **Prediction of volume of shallow landslides due to rainfall using data-driven models**

2  
3 Tuganishuri Jérémie<sup>1</sup>, Chan-Young Yune<sup>2</sup>, Gihong Kim<sup>3</sup>, Seung Woo Lee<sup>4</sup>, Manik Das Adhikari<sup>5</sup>,  
4 Sang-Guk Yum<sup>6\*</sup>

5 Department of Civil and Environmental Engineering, Gangneung-Wonju National University,  
6 \*Corresponding author: Sang-Guk Yum; [skyeom0401@gwnu.ac.kr](mailto:skyeom0401@gwnu.ac.kr)

8 **Abstract**

9 Landslides due to rainfall are among the most destructive natural disasters that cause property  
10 damages, huge financial losses, and human deaths in different parts of the World. To plan for  
11 mitigation and resilience, the prediction of the volume of rainfall-induced landslides is essential to  
12 understand the relationship between the volume of soil materials debris and their associated  
13 predictors. Objectives of this research are to construct a model by utilizing advanced data-driven  
14 algorithms (i.e., ordinary least square or Linear regression (OLS), random forest (RF), support  
15 vector machine (SVM), extreme gradient boosting (EGB), generalized linear model (GLM),  
16 decision tree (DT), ~~and~~ deep neural network (DNN), ~~K-~~nearest neighbor (KNN) and Ridge  
17 regression (RR)) for the prediction of the volume of landslides due to rainfall considering  
18 geological, geomorphological, and environmental conditions. Models were trained and tested on  
19 the Korean landslide dataset to obtain the most efficient predictions. The ~~extreme gradient~~  
20 ~~boosting~~EGB predictions exhibited optimal predictions with the highest coefficient of  
21 determination ( $R^2=0.8841$ ) and lowest mean absolute error (MAE=146.6120 m<sup>3</sup>), followed by  
22 ~~random forest ( $R^2=0.8435$ , MAE=330.4876 m<sup>3</sup>)-RF ( $R^2=0.8435$ , MAE=330.4876 m<sup>3</sup>) for the~~  
23 holdout set. The results indicated that the DNN, EGB, and RF models exhibited  $R^2>0.8$  on both  
24 the training and test sets. The difference in coefficient of determination  $R^2$  on the training and  
25 holdout set were 1.75, 7.72, and 12.17% for RF, EGB and DNN, respectively, signifying that the  
26 model could yield reliable volume estimates in adjacent areas with similar geomorphological and  
27 environmental settings. The volume of landslides was strongly influenced by slope length,  
28 maximum hourly rainfall, slope angle, aspect, and altitude. The anticipated volume of landslides  
29 can be important for land use allocation and efficient landslide risk management.

31 **Keywords:** Data-driven models, volume of landslides, ~~prediction models~~optimal predictive model,

- 서식 지정함: 글꼴 색: 자동
- 서식 있음: 금칙 처리 안 함, 단어 잘림 방지, 문장 부호 끌어 맞추지 않음
- 서식 지정함: 글꼴 색: 자동
- 서식 있음: 양쪽, 금칙 처리 안 함, 문장 부호 끌어 맞추지 않음, 한글과 영어 간격을 자동으로 조절하지 않음, 한글과 숫자 간격을 자동으로 조절하지 않음
- 서식 지정함: 글꼴 색: 자동
- 서식 지정함: 글꼴 색: 자동
- 서식 지정함: 글꼴 색: 자동
- 서식 있음: 금칙 처리 안 함, 문장 부호 끌어 맞추지 않음, 한글과 영어 간격을 자동으로 조절하지 않음, 한글과 숫자 간격을 자동으로 조절하지 않음
- 서식 있음: 간격 단락 뒤: 0 pt, 금칙 처리 안 함, 단어 잘림 방지, 문장 부호 끌어 맞추지 않음
- 서식 있음: 간격 단락 뒤: 0 pt, 단락의 첫 줄이나 마지막 줄 분리 방지, 금칙 처리 안 함, 단어 잘림 방지, 문장 부호 끌어 맞추지 않음
- 서식 지정함: 글꼴 색: 자동
- 서식 지정함: 글꼴 색: 자동
- 서식 지정함: 글꼴 색: 자동
- 서식 지정함: 글꼴 색: 자동
- 서식 지정함: 글꼴 색: 자동
- 서식 지정함: 글꼴 색: 자동
- 서식 있음: 들여쓰기: 왼쪽: 0 cm, 내어쓰기: 10.8 글자, 금칙 처리 안 함, 단어 잘림 방지, 문장 부호 끌어 맞추지 않음

32 rainfall, South Korea

33  
34 **1. Introduction**

35 Landslides due to rainfall are phenomena that dislocate a mass of soil from its natural position and  
36 slide downward along a slope due to gravity forces. Intense or long-duration rainfall infiltrates the  
37 soil and increases the pore pressure, resulting in soil saturation that leads to slope failure. The  
38 saturated soil becomes weak and loses cohesion, and the slope fails when rainfall crosses a certain  
39 threshold (Bernardie et al., 2014; Martinović et al., 2018; Lee et al., 2021). The heavy rainfall  
40 saturates a slope and triggers a landslide due to the reduction of the soil's shear strength and the  
41 increase of pore water pressure (Luino et al., 2022; Chen et al., 2021; Chatra et al., 2019; Tsai and  
42 Chen, 2010; Lacerda et al., 2014; Tsai and Chen, 2010; Chatra et al., 2019; Chen et al., 2021; Luino  
43 et al., 2022). For example, steep slopes with loose soils and even moderate rainfall can lead to the  
44 displacement of an enormous quantity of soil mass. On the contrary, in slopes with more stable,  
45 cohesive soils, the surface failure might be smaller (Tsai and Chen, 2010). The rainfall quantity  
46 and duration influence the volume of the landslides; the higher the intensity and the longer the  
47 duration of rainfall, the larger the resulting surface failure (Chen et al., 2017; Chang and Chiang,  
48 2009; Bernardie et al., 2014; Chang and Chiang, 2009; Chen et al., 2017). The landslide occurrences  
49 can also be influenced by human activities that weaken the slope, such as excavation at the slope  
50 toe and loading caused by construction and land use such as agriculture, mining etc. (Rosi et al.,  
51 2016). The rapid urbanization activities in mountainous regions affect the topography through hill  
52 cutting, deforestation and water drainage (Rahman et al., 2017); these activities disturb the slope  
53 structure and change the water flow, which exacerbates the effect of landslides in regions where  
54 human engineering activities are mostly located (Holcombe et al., 2016; Islam et al., 2017; Chen  
55 et al., 2019; Chen et al., 2019). Therefore, to mitigate landslide-induced risks in the runoff regions,  
56 estimation of the volume of landslides due to rainfall (VLDR) plays a crucial role.

57 ~~To estimate the volume of the soil mass displaceable subsequent to intensive rainfall, is~~  
58 ~~essential to set appropriate mitigation strategies to reduce environmental degradation,~~  
59 ~~infrastructure damage, casualties, and to establish post-disaster resilience policies to restore the~~  
60 ~~socio-economic aspect of communities (Van et al., 2021; Alcántara Ayala, 2021). This The~~  
61 ~~quantification of the volume of landslides due to rainfall (VLDR) is essential for effective risk~~

서식 있음: 금칙 처리 안 함, 단어 잘림 방지, 문장 부호  
끌어 맞추지 않음

서식 지정함: 글꼴 색: 자동

서식 지정함: 글꼴 색: 자동

서식 지정함: 글꼴 색: 자동

서식 지정함: 글꼴 색: 자동

서식 지정함: 글꼴 색: 자동

서식 지정함: 글꼴 색: 자동

서식 지정함: 글꼴 색: 자동

서식 지정함: 글꼴 색: 자동

서식 지정함: 글꼴 색: 자동

62 management (Tacconi Stefanelli et al., 2020), emergency response, engineering design (Cheung,  
63 2021), economic assessment and environmental protection (Alcántara-Ayala and Sassa, 2023).  
64 ~~Firstly, to manage landslide risk effectively, With the quantification estimates of VLDR, the~~  
65 ~~morphologist can be useful for updating update~~ hazard maps (Van Westen, 2000) to reflect the  
66 scale of potential ~~landslides-mass movement~~ in various regions to ~~facilitate the identification of~~  
67 ~~high-risk zones for monitoring and intervention. In addition, to develop mitigation strategies, such~~  
68 ~~as land stabilization measures and land use planning, planners might put in place strict construction~~  
69 ~~regulations in particular obtain~~ regions that are susceptible to landslides (Mateos et al., 2020). The  
70 ~~accurate measurements of VLDR can be used to promote public awareness for safety measures~~  
71 ~~and preparedness (Yang and Adler, 2008). Secondly, estimating precise VLDR is crucial for~~  
72 ~~structural-with similar likelihood of landslides of similar soil mass to highlight risk zone levels,~~  
73 ~~i.e., low, moderate and high. These classifications help engineers to design a structure that can~~  
74 ~~withstand extreme landslide events. Knowing the exact volume of displaceable material, an~~  
75 ~~engineer can set robust stabilization solutions to prevent future occurrences (Dai and Lee, 2001).~~  
76 ~~Moreover, the VLDR can help design the drainage system to manage water flow by controlling~~  
77 ~~groundwater and surface runoff to mitigate landslide risks (Dikshit et al., 2019; Kim et al., 2014).~~  
78 ~~Furthermore, to prepare for emergence responses such as resource allocation, evacuation planning,~~  
79 ~~and search and rescue operations, accurate VLDR estimation is necessary to ensure efficient~~  
80 ~~implementation (Fan et al., 2019). To allocate resources effectively, the volume data is needed to~~  
81 ~~determine the expected number of personnel for evacuation, materials sufficient for cleaning up~~  
82 ~~and recovery (Amatya, 2016; Yang and Adler, 2008; Spiker and Gori, 2003). Further, to establish~~  
83 ~~environmental protection measures such as ecosystem impacts, preservation of soil and water~~  
84 ~~quality, and habitat restoration, the estimates of VLDR are essential (Pradhan et al., 2022; Li et al.,~~  
85 ~~2022a; Barik et al. apply appropriate slope stabilization techniques depending on the level of risk~~  
86 ~~( Dahal and Dahal, 2017).~~

서식 지정함: 글꼴 색: 자동

서식 지정함: 글꼴 색: 자동

서식 지정함: 글꼴 색: 자동

서식 지정함: 글꼴: +본문(Calibri), 11 pt, 글꼴 색: 자동

서식 지정함: 글꼴 색: 자동

서식 지정함: 글꼴 색: 자동

서식 지정함: 글꼴 색: 자동

서식 지정함: 글꼴 색: 자동

서식 지정함: 글꼴 색: 자동

87 To mitigate the economic impacts of landslides, the values of VLDR can be a basis for  
88 estimation of property damages, which is critical for settling insurance claims and assessment of  
89 financial impacts on communities and government to facilitate efficient budgeting for repairing  
90 damaged infrastructure and restoration of affected parts (Klimeš et al., 2017; Dai et al., 2002). The  
91 prediction of the VLDR can assist in Additionally, enhancing the precision of VLDR estimations  
92 and improving the predictive capabilities is essential for understanding and monitoring landscape

서식 지정함: 글꼴 색: 자동

93 evolution. Montgomery (2009) emphasized that the volume of landslides is a key factor in  
94 determining the extent of downstream damage, particularly for large debris flows or rock  
95 avalanches, which can drastically alter the landscape and affect surrounding ecosystems and  
96 infrastructure. Similarly, Korup (2004) further explored the long-term economic planning for  
97 landslide risk by creating disaster preparedness and recovery funds (Winter and Bromhead, 2012).  
98 The accurate estimation of the VLDR is an important key for designing strategies for resilience  
99 and planning for the protection of the inhabitants of a particular region with certain landslide risks  
100 subjected to a predicted quantity of rainfall (Conte et al., 2022). Consequently, for the safety of  
101 communities, the selection of infrastructure construction sites must be done in places with low  
102 landslide risks (Fan et al., 2017). Further, for the protection of crops, the farmland location, and  
103 other land use activities, accurate landslide prediction taking into account real root causes through  
104 the analysis of triggering geomorphological effects of large-volume landslides, highlighting their  
105 importance in reshaping mountainous terrains, and influencing factors, is crucial to achieve a  
106 durable landslide safety management system (Paudel et al., 2003; Lee, 2009; Fan et al.,  
107 2017) sediment transport, which is critical for understanding both immediate and future landscape  
108 changes. However, the existing landslide susceptibility models mostly used for the identification  
109 of regions susceptible to landslides (i.e., landslide zonation) (Kim et al., 2014; Gutierrez-Martin,  
110 2020; Chen et al., 2019; Dai et al., 2019; Alcántara Ayala, 2021), 2021; Li et al., 2022), which are  
111 essential in emergency management because they provide a general overview of zones with a  
112 higher probability of landslide occurrence; however, they do not emphasize the determination of  
113 the approximate value of the volume of failing mass in relation to excessive rainfall events.  
114 The prediction of VLDR has gained the interest of many Numerous researchers to  
115 understand the mechanism used landslide inventory, remote sensing data and interaction numerical  
116 techniques to establish the relationship between triggering landslide geometry and aggravating the  
117 influencing factors. to determine the landslide volume quantitatively. For example, Saito et al.  
118 (2014) studied the relationship between rainfall-triggered landslides to test whether the volume of  
119 landslides across Japan that occurred between 2001 and 2011 can be directly predicted from  
120 rainfall metrics. The findings revealed that larger landslides occurred when rainfall exceeded  
121 certain thresholds, but there were significant discrepancies between peaks of rainfall metrics and  
122 maximum landslide volumes, and the total rainfall was the suitable predictor of landslides. Dai  
123 and Lee (2001) established the frequency-volume relation for landslides in Hong Kong and noticed

서식 지정함: 글꼴 색: 자동

서식 지정함: 글꼴 색: 자동

서식 지정함: 글꼴 색: 자동

서식 지정함: 글꼴 색: 자동

서식 지정함: 글꼴 색: 자동

서식 지정함: 글꼴 색: 자동

서식 지정함: 글꼴 색: 자동

서식 지정함: 글꼴 색: 자동

서식 지정함: 글꼴 색: 자동

서식 지정함: 글꼴 색: 자동

124 that the relation for shallow landslides above 4m<sup>3</sup> followed the power law. The 12-hour rolling  
125 rainfall contributed most to the prediction of the volume of landslides, [Jaboyedoff et al. \(2012\)](#)  
126 [contributed by demonstrating the value of remote sensing technologies such as Light Detection](#)  
127 [and Ranging \(LiDAR\) in conjunction with field data to improve the accuracy of volume estimates](#)  
128 [and capture the geomorphological changes associated with landslides.](#) [Ju et al. \(2023\)](#) constructed  
129 an area-volume power law model for the estimation of the volume of landslides using high-  
130 resolution LiDAR data collected between 2010 and 2020 in Hong Kong. The aim was to estimate  
131 accurately the volume of landslides on small-scale landslides. The reliance on localized datasets  
132 limits the model's applicability in regions with different geological settings, and the model does  
133 not consider all variabilities of landslide characteristics. [Razakova et al. \(2020\)](#) calculated  
134 landslide volume using remote ~~sensed~~sensing data ~~with the aim of assessing to assess~~ the efficiency  
135 of aerial photographs in environmental impact assessment and ground-based measurement. The  
136 study did not ~~take into account~~consider the effect of vegetation and topography and only focused  
137 on a single landslide case, which may be a source of bias due to differences in soil composition  
138 and environmental factors. [Hovius et al. \(1997\)](#) analyzed multiple sets of aerial photos and  
139 frequency-magnitude relations for landslides in New Zealand. The finding pinpointed that the  
140 landslides frequency-magnitude followed power law and infrequent large magnitude contributed  
141 to the landscape change. The study also noticed the importance of soil composition in the size of  
142 the landslides. This work had a limitation due to the reliance on aerial photos only, which cannot  
143 provide accurate measurement in regions of dense forest, and the climatic conditions, which are  
144 landslide triggering factors, were not considered, and this may affect the generality of the findings.  
145 [Guzzetti et al. \(2008\)](#) applied statistical methods on regional landslide inventories and antecedent  
146 rainfall data ranging between 10 min to 35 days. The findings revealed that the slope angle and  
147 soil type significantly influence landslide volume estimates, and the rainfall intensity is more  
148 important than duration. [Chatra et al., \(2019\)](#) applied numerical methods to study the effect of  
149 rainfall duration and intensity on the generation of pore pressure in the soil; the finding revealed a  
150 higher instability in loose soil compared to medium soil slopes. ~~The work only treated the~~  
151 ~~interaction of soil and rainfall without considering the environmental factors and human activity,~~  
152 ~~which might also influence mass failure. Recently, the application of GIS technologies has been~~  
153 ~~increasing in the identification of regions susceptible to landslides (landslide zonation) (Chen et~~  
154 ~~al., 2021; Gutierrez Martin, 2020; Li et al., 2022b).~~ These methods are essential in emergency

서식 지정함: 글꼴: +본문(Calibri), 11 pt, 글꼴 색: 자동

서식 지정함: 글꼴 색: 자동

서식 지정함: 글꼴 색: 자동

서식 지정함: 글꼴 색: 자동

서식 지정함: 글꼴 색: 자동

서식 지정함: 글꼴 색: 자동

155 ~~management because they provide a general overview of zones with a higher probability of~~  
156 ~~landslide occurrence; however, they do not put emphasis on the determination of the approximate~~  
157 ~~value of the volume of failing mass in relation to excessive rainfall events~~ Huang et al. (2020)  
158 ~~introduced a hybrid machine-learning model combining support vector regression (SVR) with a~~  
159 ~~genetic algorithm to estimate debris-flow volumes. The model was tested on real-world case~~  
160 ~~studies, showing improved accuracy in volume predictions compared to traditional methods.~~  
161 ~~However, a notable weakness of the study is its reliance on a limited dataset, which may reduce~~  
162 ~~the model's generalizability to environmental contexts. Shirzadi et al. (2017) compared the~~  
163 ~~effectiveness of statistical and machine-learning models in simulating landslide volumes-areal~~  
164 ~~relations, demonstrating that machine-learning techniques outperform traditional statistical~~  
165 ~~methods in terms of accuracy. This method did not consider the climatic and geomorphic factors~~  
166 ~~such as rainfall, vegetation, soil type, etc., triggering and influencing factors for the landslide~~  
167 ~~occurrence. It was noted that existing models only treated the interaction of soil and rainfall~~  
168 ~~without considering the environmental factors, human activity, and non-linear behavior of the~~  
169 ~~triggering and influencing factors.~~

170 In the present study, the volume of landslides due to rainfall is predicted using OLS, RF,  
171 SVM, EGB, GLM, DT, DNN, KNN and RR algorithms, considering the details of triggering  
172 factors (i.e., rainfall) and predisposing factors (i.e., geomorphological, soil and environmental).  
173 Here, we aim to construct a data-driven algorithm that combines input parameters for physical-  
174 based and empirical models and incorporates more complex non-linear features of input variables  
175 to predict the occurrence of associated events more accurately. The main assumption behind the  
176 data-driven algorithm is that the considered feature input of the model produces a similar volume  
177 of landslides due to rainfall and follows the same pattern at a particular region with the same  
178 features under the same quantity of rainfall. Here, we examine different machine learning (ML)  
179 algorithms and compare their performance using the coefficient of determinations ( $R^2$  and), mean  
180 square errors (MAE), Root mean square error (RMSE), Mean absolute percentage error (MAPE),  
181 and symmetric mean absolute percentage errors (SMAPE) of the predicted volume of landslides.  
182 The focus is to optimize the predictions of the volume of landslides due to rainfall, taking into  
183 account triggering and influencing factors with higher accuracy.

184  
185 **2. Data and Study Region**

서식 지정함: 글꼴 색: 자동

서식 지정함: 글꼴 색: 자동

서식 지정함: 글꼴 색: 자동

서식 지정함: 글꼴 색: 자동

서식 지정함: 글꼴 색: 자동

서식 지정함: 글꼴 색: 자동

서식 지정함: 글꼴 색: 자동

서식 있음: 금칙 처리 안 함, 단어 잘림 방지, 문장 부호  
끌어 맞추지 않음

186 **2.1. Study Region**

187 The region for testing the model is South Korea, characterized by mountainous (63% of total land)  
188 relief, especially in the eastern part of the country (Lee et al., 2022). South Korea is located on the  
189 southern part of the Korean Peninsula, bordered by the Yellow Sea to the west coast and the East  
190 Sea (Sea of Japan) to the East. According to the Korean Meteorological Administration  
191 (2020),<https://www.kma.go.kr/>, the country has a temperate climate characterized by four distinct  
192 seasons: hot and humid summers, cold winters, and springs and falls with moderate temperatures.

193 The annual rainfall ~~rangesvaries~~ between 1000 mm to ~~1400mm~~1400 mm and ~~1800mm~~1800 mm  
194 for the central region and southern region, respectively (Jung et al., 2017; Alcantara and Ahn,  
195 2020). During the summer, heavy rainfall from June to September leads to significant surface  
196 runoff, increases landslide risk, and causes approximately 95% of all landslides each year (Lee et  
197 al., 2020; Park and Lee, 2021). In addition, the landslides may be aggravated by typhoons, which  
198 mostly occur in August and September, and it is anticipated that frequency will increase due to  
199 climate change (Kim and Park, 2021). The rainfall trend analysis from 1971 to 2100 predicted

200 ~~thean~~ increase in rainfall of 271.23mm, which indicates the growing risk of landslides associated  
201 with climate change (Lee, 2016). Temperature variations are influenced by its geographical  
202 location; the average summer temperatures ~~rangevary~~ between 25 and 30°C, while winter  
203 temperatures can drop to -10°C in some parts of the country (~~Korea Meteorological~~  
204 ~~Administration, 2020)~~<https://web.kma.go.kr/>). The South Korean geologically is mainly  
205 composed of granitic and metamorphic rocks, such as gneiss, schist, and granite, which influence  
206 the stability of the landscape (Jung et al., 2024). The geomorphology is characterized by rugged  
207 mountains, river valleys, and coastal plains, with the Taebaek Mountains running along the eastern  
208 edge (Kim et al., 2020). In addition, the influence of rainfall, environmental, geomorphology, and  
209 geological factors increase the vulnerability to landslides across the country, especially in the  
210 northeastern mountainous region, as depicted in Figure 1.

211 ~~The~~ predominant soil types in South Korea include clay, sandy, and loamy soils, each with  
212 different characteristics affecting water infiltration, retention and erosion (Kang et al., 2022; Lee  
213 et al., 2023). Clay soils, being more stable, can become highly saturated, increasing landslide risk  
214 during heavy rains. On the other hand, sandy soils are more prone to shallow landslides due to fast  
215 saturation, leading to instability. Regions with steep topography and poorly consolidated soil  
216 (loose) are mostly at risk, especially after prolonged rainfalls (Kim et al., 2015).

서식 지정함: 글꼴 색: 자동

서식 지정함: 글꼴 색: 자동

서식 지정함: 글꼴 색: 자동

서식 지정함: 글꼴 색: 자동

서식 지정함: 글꼴 색: 자동

서식 지정함: 글꼴 색: 자동

서식 지정함: 글꼴 색: 자동

서식 지정함: 글꼴 색: 자동

서식 지정함: 글꼴 색: 자동

서식 있음: 들여쓰기: 첫 줄: 0 cm



217 Coastal areas are exposed to sea level rise and coastal erosion, which can further  
 218 complicate the landscape and increase landslide susceptibility. The combination of heavy summer  
 219 rainfall, geological composition, and geomorphological factors makes South Korea particularly  
 220 vulnerable to shallow landslides. Thus, continuous monitoring and research are vital to  
 221 understand the complex interactions between climate, geology, soil types, and  
 222 landslide occurrences in this region (Park, 2022). Understanding the combination of  
 223 meteorological, environmental, geological stability, and geomorphological features is crucial  
 224 for developing effective disaster management strategies and enhancing public safety in landslide-  
 225 prone areas. As climate change continues to impact rainfall patterns, South Korea faces ongoing  
 226 challenges in mitigating landslide risks and protecting vulnerable communities.

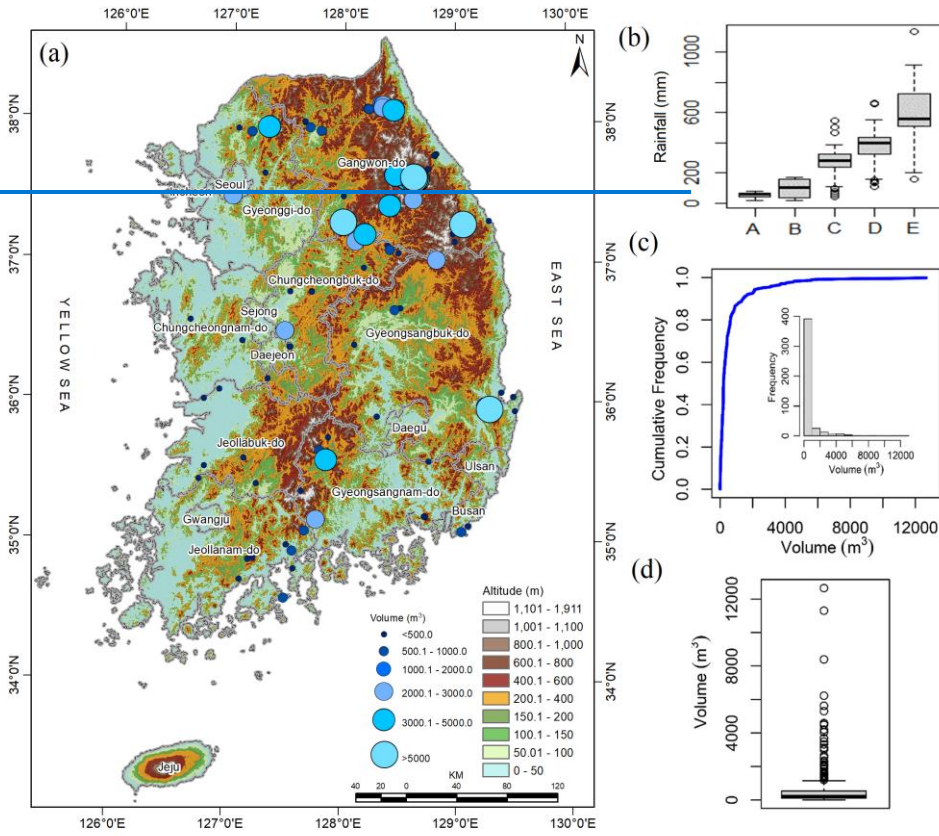
서식 지정함: 글꼴 색: 자동

서식 지정함: 글꼴 색: 자동

서식 지정함: 글꼴 색: 자동

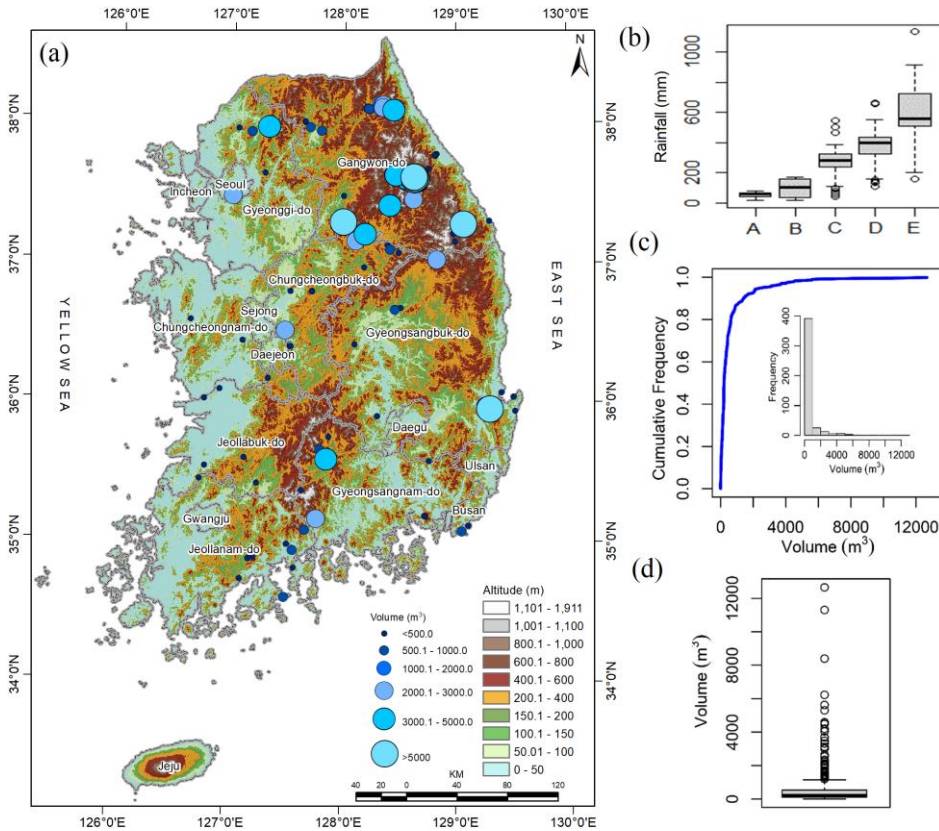
서식 지정함: 글꼴 색: 자동

서식 지정함: 글꼴 색: 자동



227





228  
 229 Figure 1. (a) Spatial distribution of landslides in South Korea, (b) ~~temporal~~Temporal variation of  
 230 rainfall, i.e., A: Maximum hourly rainfall, B: Four weeks rainfall, C: Three hours  
 231 rainfall, D: Three days rainfall and E: Two weeks rainfall, (c) ~~eumulative~~Cumulative  
 232 frequency distribution of ~~the~~ volume of landslides, and (d) ~~box~~Box plot of ~~the~~ volume  
 233 of landslides.

234  
 235 **2.2 Data**

236 The landslide inventory dataset contains 455 landslide record information from 2011 to 2012,  
 237 collected from different locations in South Korea by Korean Forest Services. This dataset tabulates  
 238 information on landslide geometry, such as runout length, width, depth, and volume of the affected

서식 지정함: 글꼴 색: 자동

서식 지정함: 글꼴 색: 자동

서식 지정함: 글꼴 색: 자동

서식 지정함: 글꼴 색: 자동

서식 지정함: 글꼴 색: 자동

서식 지정함: 글꼴 색: 자동

서식 지정함: 글꼴 색: 자동

239 area, along with geomorphological composition, vegetation, and antecedent rainfall prior to  
 240 landslide events. The details regarding landslide predisposing and triggering factors are  
 241 summarized in Table 1.

242 The majority of landslides in this region were shallow, translational slope failures (Kim  
 243 and Chae, 2009; Kim et al., 2001). The occurred landslides had a volume varying between 1.5m<sup>3</sup>  
 244 to 12,663m<sup>3</sup> and predominantly occurred in the northeastern and southeastern region (Fig. 1a,c  
 245 & d). The occurred landslides were hallowed and skewed to the right with 2570.7m<sup>3</sup> as 95<sup>th</sup>  
 246 quantile, largest volume was 12,663m<sup>3</sup>, and the aggregate mass of landslide due to rainfall was  
 247 276,986.62m<sup>3</sup>. The estimation of the volume of removed material by landslides is important as it  
 248 helps to assess risks the estimated damage can cause down at the toe of the failed slope, such as  
 249 blocking transportation network, burying crops or farmland, the damage-built environment near  
 250 landslide risks area, and post-disaster recovery planning (Evans et al., 2007; Rotaru et al., 2007;  
 251 Intrieri et al., 2019).

252  
 253 Table 1. Landslide influencing and triggering factors.

Group	Features	Description	Feature Relevance	Reference
Vegetation	Fire history	The burning of the vegetation intensifies the mass movement of soil near the uncovered burned stem of trees and free movement on uncovered soil due to post-fire rainfall and storms. The sliding may also be due to loss of vegetation, and altered soil property and structure, which lead to soil degradation and infiltration, which increase pore pressure, and change in hydrology by concentrating water flow in places that exacerbate landslides.		Highland and Bobrowsky, 2008; Stoof et al., 2012; Hyde et al., 2016; Culler et al., 2021; Hyde et al., 2016; Stoof et al., 2012
	Age of tree	Mature forests have more resistance to shallow landslides due to highly developed roots, which improve soil cohesion and leaves that prevent direct contact of raindrops with the soil surface.		Sato et al., 2023; Lann et al., 2024
	Forest density	The presence of forest reduces the likelihood of landslides about three times compared to grassland. Grassland has		Lann et al., 2024; Greenwood et al., 2004; Turner et al.,

서식 지정함: 글꼴 색: 자동

서식 지정함: 글꼴 색: 자동

서식 지정함: 글꼴 색: 자동

서식 지정함: 글꼴 색: 자동

서식 지정함: 글꼴 색: 자동

서식 있음: 한글과 영어 간격을 자동으로 조절하지 않음, 한글과 숫자 간격을 자동으로 조절하지 않음

서식 지정함: 글꼴 색: 자동

서식 지정함: 글꼴 색: 자동

서식 지정함: 글꼴 색: 자동

서식 지정함: 글꼴 색: 자동

서식 지정함: 글꼴 색: 자동

서식 있음: 한글과 영어 간격을 자동으로 조절하지 않음, 한글과 숫자 간격을 자동으로 조절하지 않음

서식 지정함: 글꼴 색: 자동

서식 지정함: 글꼴 색: 자동

서식 지정함: 글꼴 색: 자동

Group	Features	Description	Feature Relevance	Reference	References
Geomorphology		been revealed to be three times more vulnerable to shallow landslides than broadleaf and coniferous, and in secondary forests.		2010; Scheidl et al., 2020; Asada <del>et al.</del> and Minagawa, 2023; Lann et al., 2024	서식 지정함 서식 지정함 서식 있음 서식 지정함 서식 지정함 서식 지정함 서식 지정함 서식 지정함
	Timber diameter (m)	Tree spacing and size <del>had been were</del> used to investigate the effect of root and tree in shallow landslide control. The <del>high</del> High root density generally enhances slope stability, and specific tree placement and root sizes between 5 to 20 mm are effective in landslide prevention effectively prevent landslides.		Wang et al., 2016; Cohen and Schwarz, 2017; Wang et al., 2016	서식 지정함 서식 지정함 서식 지정함 서식 지정함 서식 지정함 서식 지정함
	Drainage	The drainage <del>has a significant effect on the</del> significantly affects slope stability and promotes the efficient control of the rainfall's influence of rainfall on the ground water on groundwater fluctuation. The presence of drainage increases the threshold of landslides due to rainfall.		Korup et al., 2007; Sun et al., 2010; Yan et al., 2019; Sun et al., 2010; Wei et al., 2019; Korup et al., 2007	서식 지정함 서식 지정함 서식 지정함 서식 있음 서식 지정함 서식 지정함 서식 지정함 서식 지정함
	Slope angle (degree)(°)	The steeper slopes have a lower presence of <del>landslide</del> landslides due to the low transportable materials. Slopes between 20-40 degrees are most vulnerable to greater landslides as rainfall intensity and duration increase. Here, we considered Generally, the average angle of the terrain at the landslide location, which provides valuable insight into the region's overall steepness and geomorphic characteristics, which are crucial factors influencing landslide susceptibility and risk modeling.		Donnarumma et al., 2013; Duc, 2013; Qiu et al., 2016; Donnarumma et al., 2013	서식 지정함 서식 지정함 서식 지정함 서식 지정함 서식 지정함 서식 지정함 서식 지정함 서식 지정함 서식 있음 서식 지정함 서식 지정함 서식 지정함 서식 지정함
	Slope aspect	The effect of rainfall on slope differs by slope angle and slope aspect, which <del>lead leads</del> to unevenly distributed <del>occurrence of</del> landslides.		Panday and Dong, 2021; Cellek, 2021	서식 지정함 서식 지정함
	Slope length (m)	The volume increases as the slope length increases. There exists a complex interplay exists between rainfall, length of		Turner et al., 2010	서식 지정함 서식 지정함
					서식 지정함

Group	Features	Description	Feature Relevance	Reference	References
		slope and slope angle <del>on</del> the occurrence of landslides.			
	Soil depth (m)	Soil properties, depth, and texture have significant differences in infiltration rates, which have different influences on the occurrence of landslides.		Kitutu et al., 2009; McKenna et al., 2012	
	Soil type	<del>Higher rainfall intensity affects the occurrence of landslides differently, particularly in certain soil types that have shorter saturation and failure times. Soil types, namely, Sandy loam, silt loam and loam, with their coefficient of permeability 1.7, 1.65 and 1.5, respectively, retain water differently, leading to different saturation times. The soil with higher permeability tends to drain water more efficiently, making it less prone to saturation. In contrast, the soil with lower permeability, the pore pressure rapidly increases, which leads to shallow landslide initiation during intense rainfall events.</del>		Chen et al., 2015a; Liu et al., 2021, 2021a	
Location	Altitude	Regional variability of elevation and mountain steepness affect the quantity of rainfall and associated landslides.		Um et al., 2010; Hyun et al, 2010; Yoon and Bae, 2013; Park, 2015	
	Maximum hourly rainfall	The rainfall infiltrates the slope and increases pore water pressure <del>that, which</del> reduces soil shear strength, <del>which and</del> leads to soil saturation, that causes surface failure.		Wieczorek, 1987; Smith et al., 2023; Dai and Lee, 2001; Smith et al., 2023	
Rainfall	Continuous rainfall	Sudden intense rainfall concentrated in short periods <del>of time</del> is responsible for shallow <del>landslide</del> landslides and debris flow.		Zhang et al., 2019	
	Three hours rainfall				
	Three days rainfall	The antecedent rainfalls increase moisture in the soil and weaken soil cohesion.		Ran et al., 2022; Zhang et al., 2019;	
	Two weeks rainfall			Bernardie et al., 2014; Chen et al., 2015a;	

서식 지정함: 글꼴 색: 자동

서식 지정함: 글꼴 색: 자동

서식 있음: 한글과 영어 간격을 자동으로 조절하지 않음, 한글과 숫자 간격을 자동으로 조절하지 않음

서식 지정함: 글꼴 색: 자동

서식 지정함: 글꼴 색: 자동

서식 지정함: 글꼴 색: 자동

서식 지정함: 글꼴 색: 자동

서식 지정함: 글꼴 색: 자동

서식 지정함: 글꼴 색: 자동

서식 있음: 가운데

서식 지정함: 글꼴 색: 자동

서식 지정함: 글꼴 색: 자동

서식 지정함: 글꼴 색: 자동

서식 지정함: 글꼴 색: 자동

서식 지정함: 글꼴 색: 자동

서식 지정함: 글꼴 색: 자동

서식 지정함: 글꼴 색: 자동

서식 지정함: 글꼴 색: 자동

서식 지정함: 글꼴 색: 자동

서식 지정함: 글꼴 색: 자동

서식 지정함: 글꼴 색: 자동

Group	Features	Description	Feature Relevance	Reference	References
	Four weeks rainfall			Gariano et al., 2017; Zhang et al., 2019; Ran et al., 2022.	

254

255 Location parameters such as altitude, latitude and longitude are essential elements that

256 determine the microclimate of a given region, influencing rainfall patterns (Hyun et al., 2010; Yoon

257 and Bae, 2013; Park, 2015). The northeastern region is characterized by high-elevation terrain,

258 such as [the Taebaek](#) and Sobaek ranges, which dry air and lead to orographic precipitation (Yun

259 et al., 2009). The windward mountain versants receive a substantial amount of rainfall, which can

260 increase the likelihood of landslides (Jin et al., 2022). This variation of rainfall with respect to the

261 direction highlights the importance of including slope aspect variables in landslide studies (Kunz

262 and Kottmeier, 2006). Figure 2([a](#)) depicts the relationship between the slope aspect and the

263 volume of landslides and slope aspect, altitude and fire history and shows that larger volumes were

264 localized in regions that faced forest fire and altitudes between 500 and 1000m. Additionally, the

265 topographical features such as slope length and slope angle affect the size of the landslide (Panday

266 and Dong, 2021), slope failure due to over-saturation from groundwater and rainfall infiltration

267 that destabilize the slope (Kafle et al., 2022). Furthermore, slope length, slope angle and slope

268 aspect play an important role in the determination of the volume of geological material uprooted

269 by landslides (Zaruba and Mencl, 2014; Khan et al., 2021). The slope stability depends on soil

270 composition properties, including soil permeability indices that affect water infiltration and

271 saturation level (Chen et al., 2015a). ~~From surveyed~~[In the study](#) regions, three main soil types,

272 namely, sandy loam, loam, and silt loam, were observed, and their coefficient of permeability is

273 1.7, 1.65 and 1.5, respectively (Lee et al., 2013). Moreover, to reduce the infiltration drainage

274 network that channeling rainwater terrain drains soil and reduces the saturation, which minimizes

275 the likelihood of landslide occurrence as a result of groundwater discharge and rainfall water flow

276 (Hovius et al., 1997; Wei et al., 2019). Furthermore, the vegetation protects the topsoil from the

277 direct impact of raindrops hitting the ground, which causes erosion due to the force of gravity and

278 reduces infiltration (Omweaga, 1989; Keefer, 2000). The absence of vegetation allows rainwater to

279 seep away fine topsoil, causing shallow landslides (Gonzalez-Ollauri and Mickovski, 2017). On

280 the contrary, vegetation improves soil cohesion and prevents potential shallow landslides due to

281 soil-root interaction (Gong et al., 2021; Phillips et al., 2021). The density of vegetation (forest) and

서식 지정함: 글꼴 색: 자동

서식 지정함: 글꼴 색: 자동

서식 있음: 한글과 영어 간격을 자동으로 조절하지  
않음, 한글과 숫자 간격을 자동으로 조절하지 않음

서식 지정함: 글꼴 색: 자동

서식 지정함: 글꼴 색: 자동

서식 지정함: 글꼴 색: 자동

서식 지정함: 글꼴 색: 자동

서식 지정함: 글꼴 색: 자동

서식 지정함: 글꼴 색: 자동

282 leafage type (broad, pines or mixture) directly affects the quantity of ~~raindrops~~ intercepted  
283 and prevented from directly hitting the soil, which emphasizes the ~~vegetation's contributions of~~  
284 ~~vegetation in the~~ landslides mitigation ~~role~~. Further, the occurrence of forest fires can contribute  
285 to the occurrence of landslides due to the burning of vegetation covering the area, changing soil  
286 properties and increasing soil pH (Lee et al., 2013).

287 The rainfall, a triggering factor of landslides, is the immediate cause of slope instability  
288 and failure due to infiltration that leads to saturation resulting from increased pore water pressure  
289 that reduces soil shear strength (Yune et al., 2010; Khan et al., 2012; Kim et al., 2021; Lee et al.,  
290 2021). The antecedent rainfall increases the moisture in the soil, which accelerates the soil  
291 saturation; the cumulative effect is essential to understand the saturation levels (Ran et al., 2022).

292 In this study, rainfall variables are grouped based on time, namely, continuous rainfall, which is  
293 the accumulative value of rainfall on the day of a landslide from rainfall start hour to the landslide  
294 event, maximum hourly rainfall, rainfall during the fixed period such as three hours, one day, three  
295 days, two weeks etc. (Fig. 1b). The histograms for rainfall considered in this study are depicted in  
296 Figure 2(a-f, and the b-g). The descriptive statistics for all continuous variables are illustrated in  
297 Table 2.

298

서식 지정함: 글꼴 색: 자동

서식 지정함: 글꼴 색: 자동

서식 지정함: 글꼴 색: 자동

서식 지정함: 글꼴 색: 자동, 영어(미국)

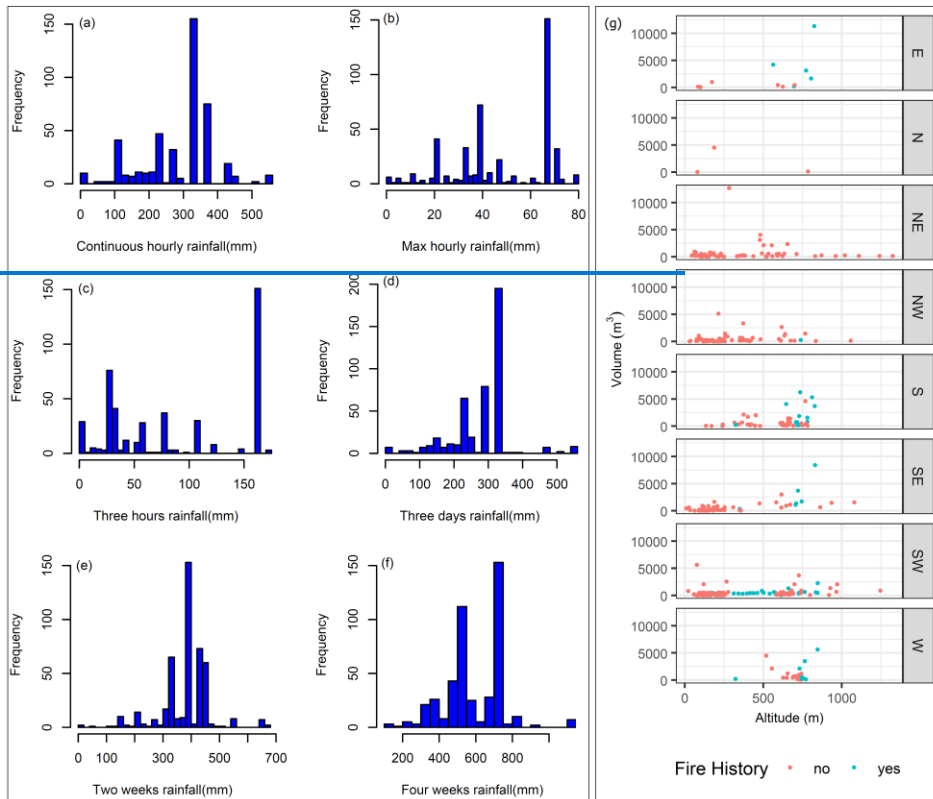
서식 지정함: 글꼴 색: 자동

서식 지정함: 글꼴 색: 자동

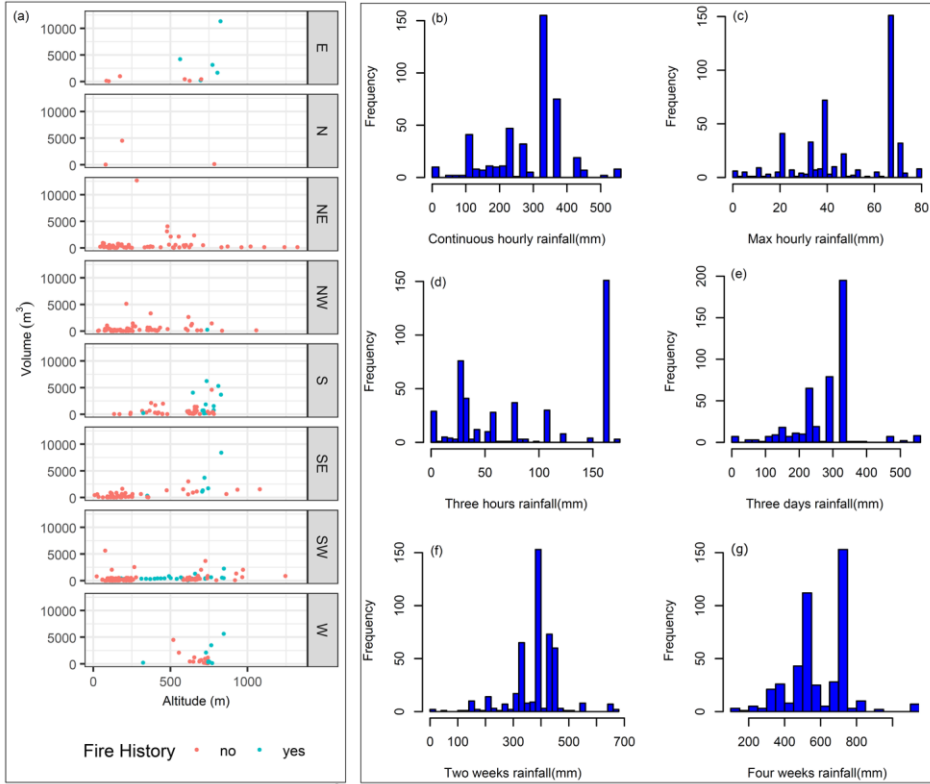
서식 지정함: 글꼴 색: 자동

서식 지정함: 글꼴 색: 자동

서식 지정함: 글꼴 색: 자동







300  
301  
302  
303  
304  
305  
306  
307  
308  
309  
310  
311  
312

Figure 2. (a-f) Histograms of rainfall data, and (g) the scatter plot showing the variation of landslide volumes with respect to slope aspect, fire history and altitude, and (b-g) Histograms of rainfall distribution.

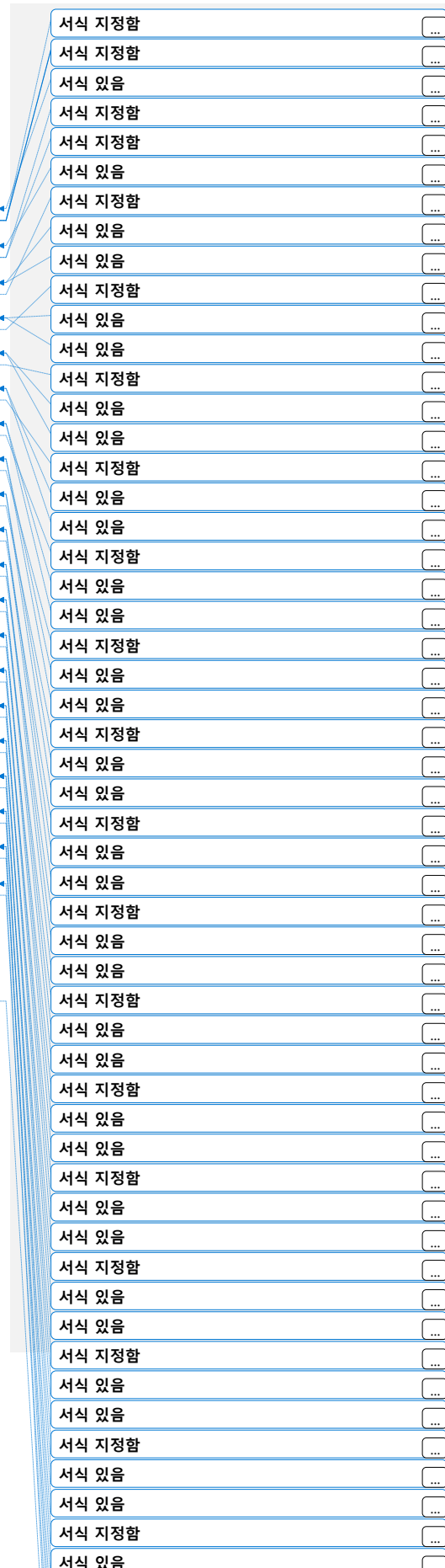
서식 지정함: 글꼴 색: 자동  
 서식 지정함: 글꼴 색: 자동  
 서식 있음: 금칙 처리 안 함, 단어 잘림 방지, 문장 부호  
 끌어 맞추지 않음  
 서식 지정함: 글꼴 색: 자동

Table 2. Summary statistics for continuous variables.

Variable	Units	N	Min	Mean	Median	Max	Std dev
Max Hourly rain	mm	455	0	48	48	78	20
Continuous rainfall	mm	455	0	285	327	550	106
Three hours rainfall	mm	455	0	88	80	171	60
Twelve Hours rainfall	mm	455	0	150	99	447	95
One day rainfall	mm	455	0	202	162	538	112
Three days rain	mm	455	0	280	284	550	86
Seven days rain	mm	455	0.5	323	330	634	88
Two weeks rain	mm	455	0.5	385	400	663	90
Three weeks rain	mm	455	86	504	533	914	115
Four weeks rain	mm	455	108	587	561	1135	160
Soil depth	m	455	0.2	0.6	0.75	0.75	0.19
Soil type	-	455	1.5	1.6	1.5	1.7	0.087
Timber diameter	m	455	0.15	0.27	0.23	0.35	0.086
Age of tree	Years	455	10	34	35	60	14
Slope length	m	455	1.8	21	13	180	23
Slope angle	Degree (°)	455	10	34	34	65	7.9
Altitude	m	455	9	391	272	1324	273

### 3. Methods

In this paper, we consider nine data-driven models, namely OLS, RF, SVM, EGB, GLM, DT, DNN, KNN and RR, to predict the volume of landslides due to rainfall. The model is tested on the South Korean landslides inventories and predisposing factors coupled with triggering factors, i.e., rainfall data. The detailed workflow is summarized in Figure 3. The steps for construction of these models can be briefly summarized as follows: a) the dataset for landslide inventories is cleaned and combined with rainfall dataset, b) the collinearity analysis is made using variance inflation factor, c) continuous feature are scaled (Z-score) (Bonamutial and Prasetyo, 2023) to facilitate algorithms to converge fast, d) the dataset is split into training and test set, e) all models are tested

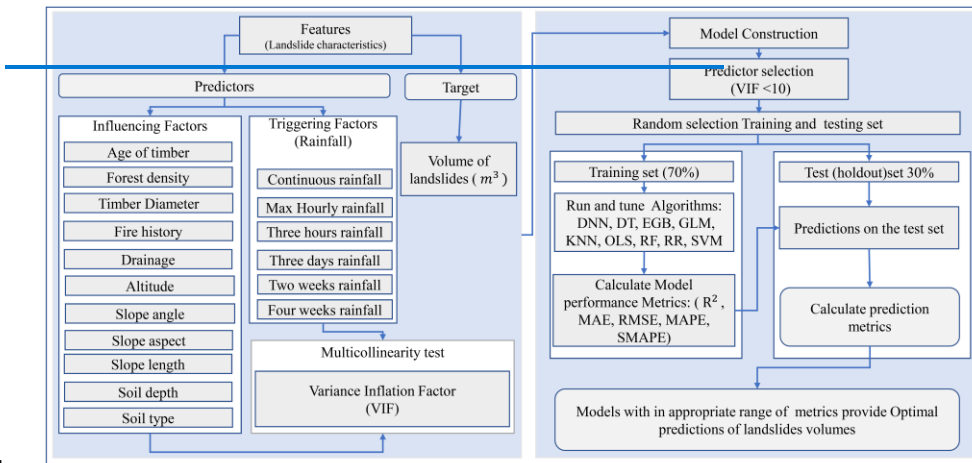


326 on the same training set, and the model evaluation on the test set using mean absolute error (MAE),  
 327 coefficient of determination ( $R^2$ ), root mean square error (RMSE), symmetric mean absolute  
 328 percentage error (SMAPE) and mean absolute percentage error (MAPE) for the comparison of  
 329 actual and predicted volume by each model, f) variable importance is calculated for most  
 330 performing the optimal model, and g) the distance correlation is calculated for each continuous  
 331 feature, and Kruskal-Wallis and Dunn test are conducted to examine the similarity of the effect of  
 332 each category on the landslide volume. ▲

서식 지정함: 글꼴 색: 자동

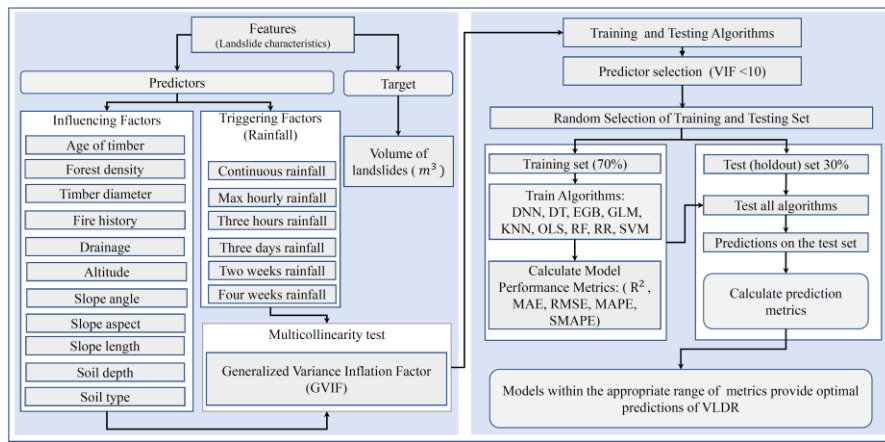
서식 지정함: 글꼴 색: 자동

333



334

335



336

337 Figure 3. Workflow for the prediction of the volume of landslides due to rainfall.

338

### 339 3.1 Model Construction

340 In the present investigation, we aimed ~~at predicting the~~ to predict landslide ~~volume of landslides~~,  
341 using models that minimize error with interpretability and scalability. Since one model can not  
342 have all properties ~~at the same timesimultaneously~~, we ~~decided to select~~ selected ~~some of the widely~~  
343 used models ~~with these~~ due to their inherent interpretability and scalability properties. The OLS,  
344 GLM, and DT were widely used for their high interpretability, which helps to understand the  
345 influence of individual features on predictions (Gelman, 2007; Breiman, 2017). On the other hand,  
346 the EGB, RF, SVM, RR, and KNN were used due to their robust performance in capturing complex  
347 patterns in data, which is essential for accurate predictions of landslide volumes (~~Chen and~~  
348 Guestrin, 2016; ~~Liaw and Wiener, 2002; Hastie, 2009; Chen and Guestrin, 2016~~). Additionally,  
349 considering that the model will be used on a regional scale, which will require big data, the EGB,  
350 RF, and DNN are designed to efficiently handle large datasets, making them suitable for the  
351 regional scale analysis. These last models can be scaled to incorporate more data from different  
352 geographical areas without significant adjustments, enhancing their applicability in future research  
353 (Krizhevsky et al., 2012). Accordingly, nine data-driven methods were selected and tested on a  
354 Korean dataset to predict VLDR.

355 The first considered method is OLS, which is applied to estimate parameters of multilinear  
356 regression that yield the minimum residual sum of squares errors from the data (~~Dismuke and~~  
357 Lindrooth, 2006 Kotsakis, 2023) under assumptions of no correlation in independent variables and  
358 ~~in~~ error term, constant variance in error terms, non-linear collinearity of predictors, and normal  
359 distribution of error terms. The RF-regression is a supervised data-driven technique based on  
360 ensemble learning, which constructs many decision trees during the training time of a model by  
361 combining multiple decision trees to produce an improved overall result of the model outcome.  
362 The RF-regression is more efficient in the analysis of multidimensional datasets (Borup et al.,  
363 2023). RF is an effective predictive model due to non-overfitting characteristics based on the law  
364 of large numbers (Breiman, 2001). The ~~decision tree (DT)~~ regression is a predictive modeling  
365 technique in the form of a flowchart-like tree structure that includes all possible results, output,  
366 predictor costs, and utility. The DT simplifies the decision-making due to its algorithm that  
367 ~~mimic~~ mimics human brain decision-making patterns (Rathore and Kumar, 2016). The KNN

서식 지정함: 글꼴 색: 자동

서식 있음: 금칙 처리 안 함, 단어 잘림 방지, 문장 부호  
끌어 맞추지 않음

서식 지정함: 글꼴 색: 자동

서식 지정함: 글꼴 색: 자동

서식 지정함: 글꼴 색: 자동

서식 지정함: 글꼴 색: 자동

서식 지정함: 글꼴 색: 자동

서식 지정함: 글꼴 색: 자동

서식 지정함: 글꼴 색: 자동

서식 지정함: 글꼴 색: 자동

서식 지정함: 글꼴 색: 자동

서식 지정함: 글꼴 색: 자동

서식 지정함: 글꼴 색: 자동

서식 지정함: 글꼴 색: 자동

서식 지정함: 글꼴 색: 자동

368 technique draws an imaginary boundary in which prediction outcomes are allocated as the average  
369 of  $k$ -nearest point predictors and averaging their output variable (response). The KNN calculates  
370 Euclidian distances to identify the likeness between datapoints, and then it groups points that have  
371 smaller distances between them (Kramer and Kramer, 2013). The RR is an improved form of  
372 ordinary least squares, which serves to respond to cases where collinearity is found in  
373 predictor variables. The estimated coefficients of ridge are biased estimators of true coefficients  
374 and are generated after adding a penalty on the OLS model. The RR has always lower variances  
375 compared to OLS (Saleh et al., 2019). The advantage of the GLM over OLS is that the dependent  
376 variable need not follow the normal distribution. The GLM is composed by random and systematic  
377 components, and the link function that links the two. In this study, the GLM with Gaussian link  
378 function was applied. GLM are fitted using maximum likelihood estimation (Dobson and  
379 Barnett, 2018). The DNN are among data-driven models that revolutionized different fields; the  
380 DNN learns via multi-processing layers and identifies intricate patterns in the data to predict the  
381 outcome (LeCun et al., 2015). Here, the backpropagation algorithm was used to predict the  
382 estimated outcome. The advantage of DNN is that it can discover the complex structures in the  
383 data using a back propagation algorithm with the capability to change capable of changing the  
384 internal parameter (weight update). The SVM is popular for balanced predictive performance  
385 which makes it capable to train model on small sample size (Pisner and Schnyer, 2020).  
386 Subsequently, SVM has been applied in many different landslide studies (Pham et al., 2018; Miao  
387 et al., 2018). SVM methods identify the optimal hyperplane in multidimensional space that  
388 separates different groups in the output values. The EGB is the most powerful and leading  
389 supervised machine learning method in solving regression problems. It can perform parallel  
390 processing on Windows and Linux (Chen et al., 2015b). The gradient boosting trains of  
391 differentiable loss function, and the model fits when the gradient is minimized. In this paper, both  
392 traditional statistical predictive models and machine learning ML models were used. The firsts are  
393 known for high clarity and explainability, and the second is famous for handling non-linearity in  
394 features. In some cases, the performance of advanced data-driven algorithms is almost similar  
395 (Chowdhury et al., 2023).

396  
397 **3.2 Feature ~~selection~~ Selection, and ~~data splitting~~ Data Splitting**

398 The variable selection procedure was carried out based on previous literature and applied

서식 지정함: 글꼴: 기움임꼴, 글꼴 색: 자동

서식 지정함: 글꼴 색: 자동

서식 지정함: 글꼴 색: 자동

서식 지정함: 글꼴 색: 자동

서식 지정함: 글꼴 색: 자동

서식 지정함: 글꼴 색: 자동

서식 지정함: 글꼴 색: 자동

서식 지정함: 글꼴 색: 자동

서식 지정함: 글꼴 색: 자동

서식 지정함: 글꼴 색: 자동

서식 지정함: 글꼴 색: 자동

서식 지정함: 글꼴 색: 자동

서식 지정함: 글꼴 색: 자동

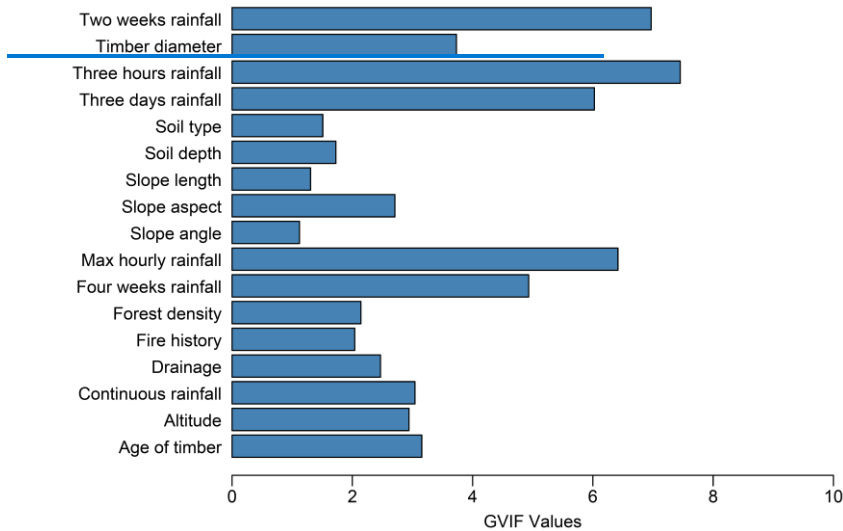
서식 지정함: 글꼴 색: 자동

서식 지정함: 글꼴 색: 자동

399 in the model using generalized variance inflation factor (GVIF) (O'Brien, 2007) to eliminate  
400 collinear variables. The variable with  $GVIF < 10$  was considered non-collinear and used in the model.  
401 Figure 4 depicts retained features and corresponding GVIF values. The retained features have  
402 GVIF less than 10 (O'Brien, 2007). Accordingly, all depicted variables were considered for the  
403 model training. Further, to train the model, the datasets were split randomly, with 70% of the data  
404 for the training set and 30% for testing (Nguyen et al., 2021). The 10-fold cross-validation was  
405 performed to obtain an optimal model.

406 The training and test set was scaled (Z-score or variance stability scaling) to solve  
407 convergence issues that are associated with running the model without feature scaling (Singh and  
408 Singh, 2022). To run the model on the data using driven methods that accept numerical features  
409 only, the test and training set was one-hot-encoded to create a feature matrix (Seger, 2018).

서식 지정함: 글꼴 색: 자동  
서식 있음: 금칙 처리 안 함, 단어 잘림 방지, 문장 부호  
끌어 맞추지 않음



410  
411

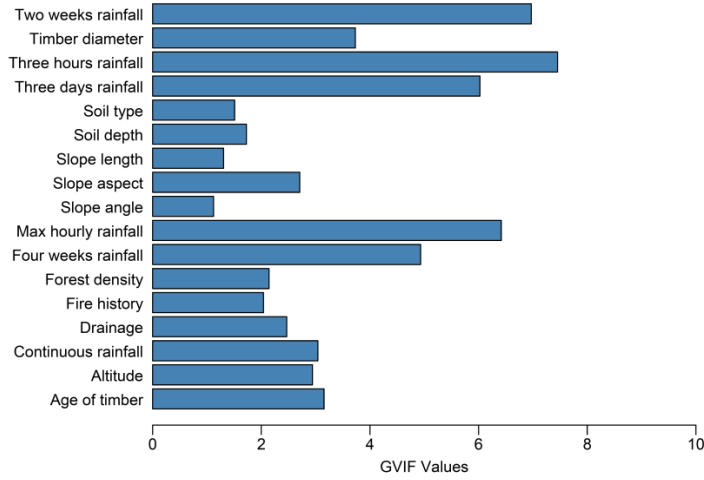


Figure 4. Generalized Variance Inflation Factor (GVIF) bar plot for features.

### 3.3 Model evaluation metrics Evaluation Metrics

The model performance evaluation is a process of quantifying the difference between the observed value not used in the modeling process and the predicted value by the model. Different metrics are applied depending on the type of task, whether it is a classification or a regression problem. Subsequently, the widely used evaluation metrics for regression models, namely,  $R^2$ , MAE, RMSE, MAPE and SMAPE, were utilized to evaluate the model performances. The metric formulae and evaluation criteria are summarized in Table 3.

Table 3. Model evaluation metrics.

Metrics	Evaluation	ReferenceReferences
$RMSE = \sqrt{\frac{1}{n} \sum_{i=1}^n (y_i - \hat{y}_i)^2}$	<ul style="list-style-type: none"> <li>Measures the square root of the average squared differences between predicted and actual values.</li> <li>Lower values indicate better model performance.</li> </ul>	Hyndman and Koehler, 2006
$MAE = \frac{1}{n} \sum_{i=1}^n  y_i - \hat{y}_i $	<ul style="list-style-type: none"> <li>The average of the absolute differences between predicted and actual values.</li> <li>Lower values indicate better model performance.</li> </ul>	Willmott and Matsuura, 2005

Vertical sidebar containing a list of 25 items, each with a text label and a small icon (three dots in a square):

- 서식 지정함
- 서식 있음
- 서식 지정함
- 서식 있음
- 서식 있음
- 서식 지정함
- 서식 지정함
- 서식 있음
- 서식 지정함
- 서식 있음
- 서식 지정함
- 서식 있음
- 서식 지정함
- 서식 지정함
- 서식 지정함
- 서식 지정함
- 서식 지정함
- 서식 지정함
- 서식 지정함
- 서식 지정함
- 서식 지정함
- 서식 지정함
- 서식 지정함
- 서식 지정함
- 서식 있음



Metrics	Evaluation	ReferenceReferences
$MAPE = \frac{100}{n} \sum_{i=1}^n \frac{ y_i - \hat{y}_i }{ y_i }$	<ul style="list-style-type: none"> <li>Measures the accuracy of a model as a percentage, which can be more interpretable.</li> <li>Lower values indicate better model performance.</li> <li>Unlike MAPE, which can be skewed by very small actual values, SMAPE accounts for both the actual and predicted values, making it symmetric.</li> <li>SMAPE is expressed as a percentage</li> <li>Mitigates the impact of small actual values on the error metric, providing a more balanced assessment.</li> <li>Lower values indicate better model performance.</li> </ul>	Armstrong, 2001
$SMAPE = \frac{100}{n} \sum_{i=1}^n \frac{ y_i - \hat{y}_i }{ y_i  +  \hat{y}_i }$	<ul style="list-style-type: none"> <li>Represents the proportion of variance in the dependent variable that can be explained by the independent variables.</li> <li>Values closer to 1 indicate a better fit</li> </ul>	Hyndman and Koehler, 2006
$R^2 = 1 - \frac{\sum_{i=1}^n (y_i - \hat{y}_i)^2}{\sum_{i=1}^n (y_i - \bar{y})^2}$		Darlington, 1990; Chicco et al., 2021

\* $y_i$  and  $\hat{y}_i$  representing the actual and predicted value and,  $\bar{y}$  and  $n$  standing for the mean of actual value and number of observations in the dataset, respectively.

#### 4. Results

The model was developed in R with different libraries, as discussed below. The DNN regression model was constructed using `dnn()` function from the `cito` library (Amesoeuder et al., 2023), with two hidden layers of (50, 50) nodes. The model was trained on 1500L epochs, learning rate (`lr = 0.01`), and loss = "mae". The [decision treeDT](#) regression model was constructed with `tree()` function from the `tree` library, with the recursive-partition method. The [ridge regressionRR](#) model was constructed using `glmnet()` function from the `glmnet` library package (Friedman et al., 2010), with ridge penalty (`alpha=0`). The optimal lambda was obtained by performing 10-fold cross-validation. The EGB model was built using `xgboost()` function in `xgboost` package (Chen et al., 2022). The optimal model was obtained at 524<sup>th</sup> boosting iteration with max depth = 5 and other parameters set to default. The GLM regression model was constructed using `glm()` function (R core Team, 2022) with family Gaussian and log link to constrain the model of predicting positive outcomes. The KNN regression was constructed using `knnreg()` function from the `caret`

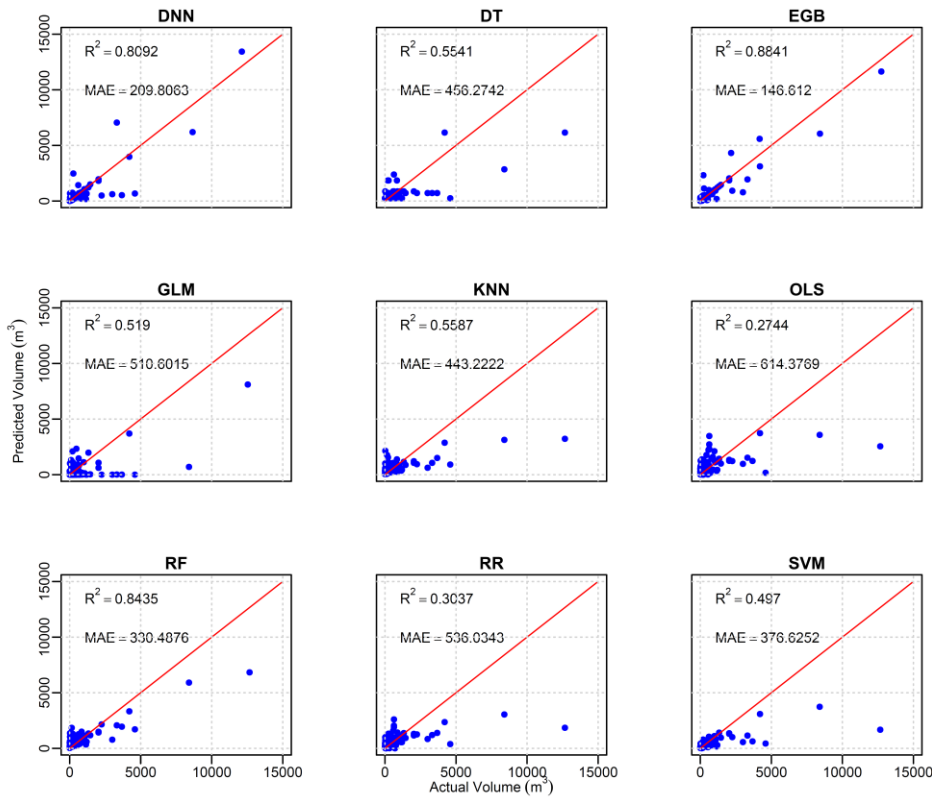
- 서식 지정함: 글꼴 색: 자동
- 서식 있음: 금칙 처리 안 함, 문장 부호 끌어 맞추지 않음, 한글과 영어 간격을 자동으로 조절하지 않음, 한글과 숫자 간격을 자동으로 조절하지 않음
- 서식 지정함: 글꼴: 11 pt, 글꼴 색: 자동
- 서식 지정함
- 서식 지정함: 글꼴 색: 자동
- 서식 있음: 금칙 처리 안 함, 문장 부호 끌어 맞추지 않음, 한글과 영어 간격을 자동으로 조절하지 않음, 한글과 숫자 간격을 자동으로 조절하지 않음
- 서식 지정함: 글꼴 색: 자동
- 서식 지정함: 글꼴 색: 자동
- 서식 있음: 금칙 처리 안 함, 문장 부호 끌어 맞추지 않음, 한글과 영어 간격을 자동으로 조절하지 않음, 한글과 숫자 간격을 자동으로 조절하지 않음
- 서식 지정함: 글꼴: 11 pt, 글꼴 색: 자동
- 서식 지정함
- 서식 지정함
- 서식 지정함: 글꼴 색: 자동
- 서식 있음: 금칙 처리 안 함, 문장 부호 끌어 맞추지 않음, 한글과 영어 간격을 자동으로 조절하지 않음, 한글과 숫자 간격을 자동으로 조절하지 않음
- 서식 지정함: 글꼴 색: 자동
- 서식 지정함
- 서식 지정함
- 서식 있음: 금칙 처리 안 함, 단어 잘림 방지, 문장 부호 끌어 맞추지 않음
- 서식 있음: 금칙 처리 안 함, 문장 부호 끌어 맞추지 않음, 한글과 영어 간격을 자동으로 조절하지 않음, 한글과 숫자 간격을 자동으로 조절하지 않음
- 서식 지정함

440 package (Kuhn, 2022), with number of neighbors,  $k=17$ . The OLS model was constructed `lm()`  
441 from the stats package (R core Team, 2022). The RF model was run using `randomForest()` from  
442 the randomforest package (Liaw and Wiener, 2002) with default parameters and the optimal model  
443 was reached at 256<sup>th</sup> iteration. ~~The ridge regression model was constructed using `glmnet()` from~~  
444 ~~the `glmnet` package (Friedman et al., 2010), with ridge penalty (`alpha=0`).~~The SVM regression  
445 model with linear kernel was built using `e1071` package (Meyer et al., 2021) and other parameters  
446 set to default.

서식 지정함: 글꼴 색: 자동

447 The predictive performance of all tested models on the holdout dataset is depicted by the  
448 scatterplot (Fig. 5) of actual volume as recorded in the test set and predicted outcome values of  
449 each model. The red line represents the perfect prediction. The scatter plot of actual and predicted  
450 values of tested models shows that OLS performed least compared to other models with  
451  $R^2=0.2744$ , that is, ~~29.27%~~ of variances in the model were explained by predictors. The second  
452 least performing was the RR with  $R^2= 0.3034$ , which is 3.6% improvement compared to OLS.  
453 Among all models, three out of nine, namely, OLS, SVM, and RR, performed below 50%;  
454 however, these models predicted well small values of volume (below 2000m<sup>3</sup>). The MAE of these  
455 three models was higher than the remaining six models, namely DNN, DT, GLM, KNN, RF, and  
456 EGB. Among these lasts, the most performing was EGB with  $R^2= 0.88$  of variance explained by  
457 predictors and MAE=146.6 m<sup>3</sup>. The evaluation metrics for the training and tested models are  
458 summarized in Table 4. Considering the  $R^2$ , the three models, namely EGB, RF, and DNN, had a  
459 value of  $R^2$  above 80% on the holdout set.

서식 지정함: 글꼴 색: 자동



서식 지정함: 글꼴 색: 자동

서식 지정함: 글꼴 색: 자동

460

Figure 5. Scatterplot of actual and predicted values for the nine tested models.

서식 지정함: 글꼴 색: 자동

462

463

464

465

466

467

468

469

470

471

472

Regarding the prediction on the training set, the GLM had an  $R^2$  of 83%. Nevertheless, the prediction on the holdout set was 51.9%; this large variation in variance explained by predictors indicates that the GLM model did not catch all non-linear patterns in the holdout set. ~~It is noteworthy that~~ Notably, the prediction difference in  $R^2$  on both training and test for the random forest exhibited a very small difference compared to EGB and DNN, that is, 1.75% compared to 12.17% and 7.72% for DNN and EGB, respectively. Despite the stable prediction of RF, the performance in terms of SMAPE, the DNN was the second lowest symmetric mean absolute percentage error,  $43.83\text{m}^3$  and  $39.79\text{m}^3$  on training and test sets, respectively. According to Chicco et al. (2021), the  $R^2$  is more informative in regression modeling; thus, RF had better predictions than the DNN.

서식 지정함: 글꼴 색: 자동

473

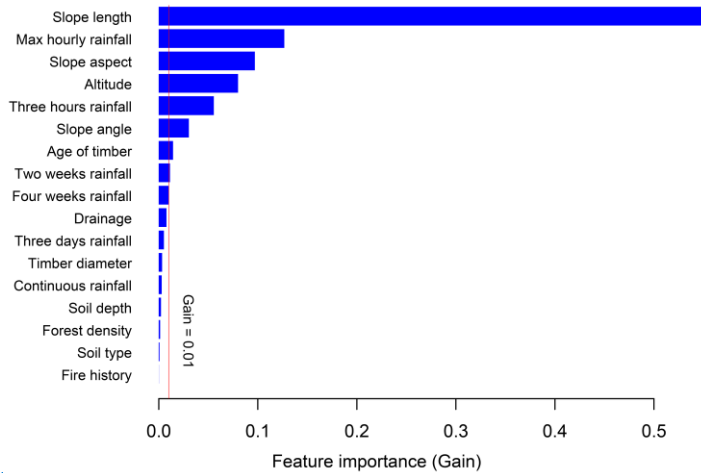
474 Table 4. Summary of prediction metrics for tested models on the training and test set.

Metrics		Models								
		DNN	DT	EGB	GLM	KNN	OLS	RF	RR	SVM
R <sup>2</sup>	Train	0.9309	0.4514	0.9613	0.8380	0.3470	0.3775	0.8610	0.3382	0.5510
	Test	0.8092	0.5822	0.8841	0.5190	0.5587	0.2744	0.8435	0.3037	0.4970
MAE	Train	132.7429	407.0814	75.1250	308.9700	410.2945	502.0053	236.9516	470.1633	276.2000
	Test	209.8063	435.5836	146.6120	510.6015	443.2222	614.3769	330.4876	536.0343	376.6252
RMSE	Train	348.6190	940.4850	113.4940	570.0070	1027.3730	1001.7620	574.9720	1042.9110	916.5471
	Test	646.5438	1047.4880	501.8960	1055.9190	1115.5270	1234.1220	737.0857	1237.9420	1176.9410
MAPE	Train	0.5240	0.7930	0.1540	76.3530	0.6280	5.2310	0.3810	1.5330	1.1588
	Test	0.5623	0.8892	0.3132	1819.2220	0.6623	4.1277	0.4939	5.8428	1.0421
SMAPE	Train	43.8375	79.8680	13.1780	150.4262	67.4715	103.0555	52.3359	93.4002	67.3221
	Test	39.7998	81.4539	22.7237	152.4991	73.6498	106.9756	63.7582	93.9244	76.9794

475

476 To dive deep into the prediction performance of the EGB model, we analyzed variables  
477 importance in the prediction of the volume. It was observed that slope length was the most  
478 contributing predictor in the performance of the EGB model, followed by maximum hourly rainfall  
479 and slope aspect. The altitude, three hours rainfall, slope angle and age of timber contributed  
480 moderately ~~into~~ the prediction of the outcome volumes with gain above 0.01 and less than 0.2.  
481 ~~the~~The antecedent rainfall from three days and above and continuous rainfall had a minor  
482 contribution, with a gain of less than 0.01 for each. The presence of rainwater drainage channels  
483 had a moderate contribution, with a gain close to 0.01. On the other hand, the contribution of soil  
484 depth and forest density in the models was insignificant and far below 0.01. Though Figure 2(~~ea~~)  
485 depicted the association between larger volumes and fire history, the variable importance indicates  
486 that the relation was not significant. Even though some variables had minor contributions,  
487 depending on the case, the contribution of those variables may also increase depending on other  
488 regional settings. Therefore, all variables with ~~Generalized variance inflation factors~~GVIF below  
489 10 were kept in the model. Figure 6 illustrates the variables importance for the EGB model. The  
490 vertical red line split the variables into two groups, the first containing variables that contributed  
491 a gain above 0.01 and others with minor contributions.

- 서식 지정함: 글꼴 색: 자동
- 서식 있음: 금칙 처리 안 함, 문장 부호 끌어 맞추지 않음, 한글과 영어 간격을 자동으로 조절하지 않음, 한글과 숫자 간격을 자동으로 조절하지 않음
- 서식 지정함: 글꼴 색: 자동
- 서식 지정함: 글꼴 색: 자동, 위 첨자
- 서식 지정함: 글꼴 색: 자동
- 서식 있음: 금칙 처리 안 함, 문장 부호 끌어 맞추지 않음, 한글과 영어 간격을 자동으로 조절하지 않음, 한글과 숫자 간격을 자동으로 조절하지 않음
- 서식 지정함: 글꼴 색: 자동
- 서식 있음: 금칙 처리 안 함, 문장 부호 끌어 맞추지 않음, 한글과 영어 간격을 자동으로 조절하지 않음, 한글과 숫자 간격을 자동으로 조절하지 않음
- 서식 지정함: 글꼴 색: 자동
- 서식 있음: 금칙 처리 안 함, 문장 부호 끌어 맞추지 않음, 한글과 영어 간격을 자동으로 조절하지 않음, 한글과 숫자 간격을 자동으로 조절하지 않음
- 서식 지정함: 글꼴 색: 자동
- 서식 있음: 금칙 처리 안 함, 문장 부호 끌어 맞추지 않음, 한글과 영어 간격을 자동으로 조절하지 않음, 한글과 숫자 간격을 자동으로 조절하지 않음
- 서식 지정함: 글꼴 색: 자동
- 서식 지정함: 글꼴 색: 자동
- 서식 지정함: 글꼴 색: 자동
- 서식 지정함: 글꼴 색: 자동



서식 지정함: 글꼴 색: 자동  
 서식 지정함: 글꼴 색: 자동  
 서식 있음: 금칙 처리 안 함, 단어 잘림 방지, 문장 부호  
 끌어 맞추지 않음

492

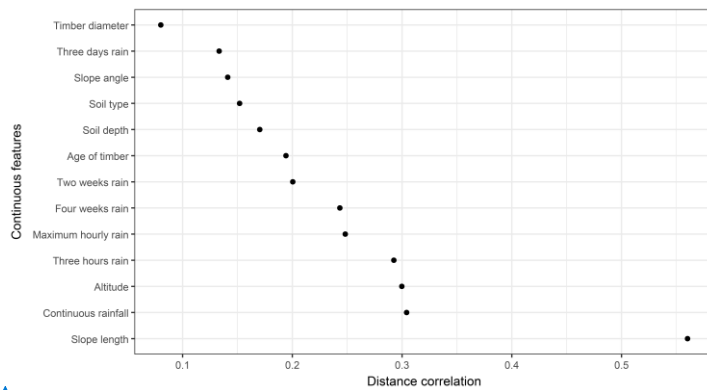
493 Figure 6. Variable importance for the EGB model.

494

495

496 The variable importance plot depicts the overall contribution of a given variable; however,  
 497 it does not provide detailed information. To get more insight into the relationship between the  
 498 volume of landslides and predictors, statistical tests for normality, namely, Shapiro-Wilk's test,  
 499 and Dunn's test were conducted. The Shapiro-Wilk's test (Dudley, 2023) results revealed that the  
 500 distribution of volume was non-normal ( $W = 0.40642$ ,  $p\text{-value} < 0.001$ ). Noting that the volume  
 501 distribution was non-normal, we opted for the non-parametric tests, which do not rely on normality  
 502 to conduct the distance correlation (Székely et al., 2007) test (dcor) for continuous independent  
 503 features. Figure 7 illustrates that the slope length exhibited a higher value (dcor=0.56) followed  
 504 by continuous rainfall altitude and three hours rainfall and kept decreasing up to timber diameter  
 505 with a distance correlation of 0.08. Overall, the distance correlation between the volume of  
 506 landslides shows a moderate strength of association between continuous predictors.

506



서식 지정함: 글꼴 색: 자동

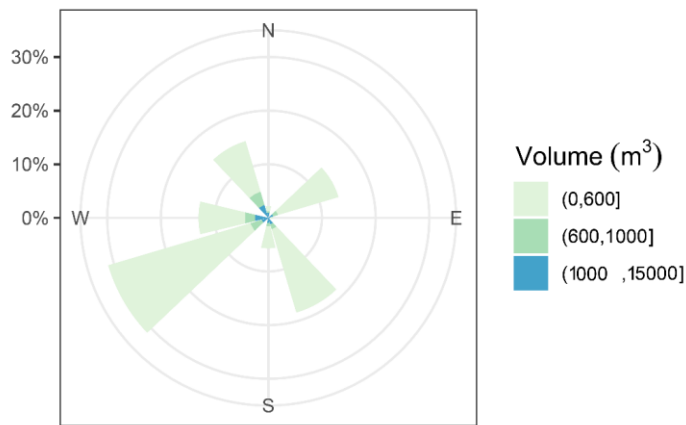
서식 지정함: 글꼴 색: 자동

507

508 Figure 7. Distance correlation plot for the volume and continuous features.

509

510 Furthermore, to test for categorical features, Kruskal-Wallis test (McKight and Najab,  
 511 2010) was used to check whether the volume of the landslide was different in each category and  
 512 Dunn's tests (Dinno, 2015) were applied to examine which categories had similar means of the  
 513 volume of landslides due to rainfall in different categories. The  $H_0$  (null hypothesis) was that the  
 514 mean volume of landslides in different categories is the same, and the  $H_1$  (alternative hypothesis)  
 515 was that the means of landslides are different in some categories. For the slope aspect, the second  
 516 most significant predictor for the EGB model, the results of Kruskal-Wallis test (chi-squared =  
 517 20.889,  $df = 7$ ,  $p$ -value = 0.003938) showed that there is a significant difference in median of  
 518 volume in some categories of slope aspects. To know which classes of slope aspects had  
 519 significantly different mean volumes, the Dunn's test results at 95% confidence interval, pairs  
 520 (East-South west, East-South East, East-South, East-North West and North West-South East) had  
 521 significantly different means of landslides' volume (with  $p$ -value < 0.05). Figure 8 depicts that the  
 522 southwest and southeast aspects had a higher frequency of landslides.



서식 지정함: 글꼴 색: 자동

서식 지정함: 글꼴 색: 자동

523  
524 Figure 8. The distribution of the volume of landslides due to rainfall with respect to the slope  
525 aspect.  
526

527 The Kruskal-Wallis test for the difference in mean of drainage classes showed the result  
528 was: chi-squared = 15.792, df = 2, p-value = 0.000372, which shows that the means of volume per  
529 class were different. This was clarified by Dunn's test results, ~~were~~ p-values were less than 0.05  
530 in all pairwise mean difference comparisons. The results of these tests highlighted that drainage  
531 has a remarkable influence on the occurrence of rainfall-induced landslides in the Korean  
532 Peninsula.

서식 지정함: 글꼴 색: 자동

533  
534 **5. Discussion**  
535 This study aim was to construct a data-driven algorithm that predicts the volume of landslides due  
536 to rainfall. Numerical models have traditionally been employed due to their foundation in physical  
537 principles such as slope stability and hydrological dynamics (Glade et al., 2005). These models are  
538 valuable for understanding the underlying mechanisms of landslide processes but often face  
539 limitations when applied to regions with complex or heterogeneous terrain, as they require  
540 detailed, high-quality input data that may not always be available (Caine, 1980). In the same way,  
541 statistical models, which use historical rainfall and landslide data to establish correlations, can  
542 offer useful predictions of VLDR in regions with extensive historical records (Chung and Fabbri,  
543 2003). However, these models may struggle to account for local variations in topography or rapidly  
544 changing weather patterns, limiting their general applicability. Additionally, ML techniques have



545 [shown significant promise in improving predictive accuracy at the regional level due to the](#)  
546 [capability of processing large, diverse datasets and capturing complex, non-linear relationships](#)  
547 [that traditional models might fail to capture \(Pourghasemi and Rahmati, 2018\). Further, ML](#)  
548 [models can adapt to regional variations and continuously improve as new data is introduced,](#)  
549 [offering a more flexible and dynamic approach to predict VLDR on a regional scale \(Liu et al.,](#)  
550 [2021b\). Subsequently, the aim of this study was to construct a data-driven algorithm that accurately](#)  
551 [predicts the VLDR.](#) The result of nine different tested algorithms revealed a tremendous difference  
552 between classical regression models (OLS, RR, and GLM) and other data-driven machine learning  
553 models. In this study, apart from SVM regression, DT and KNN, other machine learning models  
554 (DNN, DT, RF, and EGB) exhibited high prediction capability with  $R^2$  above 50% (Fig. 5). [The](#)  
555 [DNN, EGB, and RF models achieved  \$R^2 > 0.8\$  on both training and test set with accuracy reduced](#)  
556 [by 1.75, 7.72, and 12.17% for RF, EGB and DNN respectively, on the holdout set, indicating](#)  
557 [that the model could yield reliable volume estimates in adjacent areas with similar geological and](#)  
558 [environmental conditions.](#) The random forest model performed well in predicting smaller volume;  
559 however, as the volume increased, the model underpredicted volume values. The DNN model  
560 performed quite well with low MAE compared to random forest; however, the model did not  
561 perform well on moderate volume values, resulting in reduced  $R^2$ . The EGB model tested on South  
562 Korean landslide inventory coupled with rainfall data at the time of landslide events and antecedent  
563 rainfall within one month of the event exhibited [the highest performance](#) [more accurate predictions](#)  
564 compared to other constructed algorithms. The difference in performance may be due to the  
565 internal structure of each algorithm; the RF [builds](#) [multiple decision trees and averages](#)  
566 [predictions to improve accuracy \(Breiman, 2001\), while the EGB builds sequential trees in a](#)  
567 [recursive order where the new built tree improves error occurred while building the previous](#)  
568 [decision tree and optimizes the loss function through a gradient descent \(Chen and Guestrin, 2016\).](#)

569 The slope aspect played an important role in the prediction of the volume, and the landslide  
570 mostly occurred in locations oriented toward south-southwest and southeast. That may be due to  
571 the direction taken by typhoons, which hit the southwest versants of mountains upon landfall on  
572 the Korean peninsula toward the North East Pacific (Ha, 2022; Lee et al., 2013; Ha, 2022). The  
573 findings of this research are congruent with those of Lee et al. (2013), who also highlighted that  
574 the mountain versant oriented to strong wind direction may face more landslides. The study also  
575 highlighted that a moderate rainwater drainage channel plays an important role in the prevention

서식 지정함: 글꼴 색: 자동

서식 지정함: 글꼴 색: 자동

서식 지정함: 글꼴 색: 자동

서식 지정함: 글꼴 색: 자동

서식 지정함: 글꼴 색: 자동

서식 지정함: 글꼴 색: 자동

서식 지정함: 글꼴 색: 자동

서식 지정함: 글꼴 색: 자동

서식 지정함: 글꼴 색: 자동

서식 지정함: 글꼴 색: 자동

서식 지정함: 글꼴 색: 자동

576 of landslides due to its stabilizing effect. The landslide location and pattern follow the rainfall  
577 climate scenario, which highlighted a higher intensity of rainfall in the northeastern region of South  
578 Korea (Lee, 2016).

579 ~~The~~In addition, the findings of this study are congruent with Zhang et al. (2019)  
580 observations that highlighted the low influence of soil type in landslide modeling and the  
581 maximum rainfall and cumulative three hours of rainfall were the most contributing rainfall, which  
582 indicated that these shallow landslides may have been triggered by sudden rainfall concentrated in  
583 few hours before the occurrence of the event. The occurrence of landslides triggered by rainfall is  
584 a complex phenomenon that involves many interrelated environmental settings, human activity,  
585 geological conditions and climatic conditions. Moreover, the occurrence of typhoons is known to  
586 aggravate the landslides impacts on communities (Chang et al., 2008); incorporating typhoon  
587 variables in future studies to customize for regional settings may improve the accuracy of the  
588 model. The advantage of his research is that the constructed model has high predictive accuracy  
589 and can handle the non-linearity of predisposing factors. The model came to fill the gap ~~of~~in a few  
590 literatures related to the prediction of the volume of landslides using data-driven techniques. This  
591 model can be a good tool to help policy-makers ~~to~~integrate the landslides volume risks in ~~in~~  
592 policy to protect infrastructure and inhabitants dwelling near the foot of mountains with high risks  
593 of being buried by geological materials resulting from landslides.

594 ~~To~~ understand the applicability of the developed models, the trained model was tested  
595 using unknown data (test data), with volume predictions generated solely based on the predictor  
596 variables; actual volume values were utilized only for evaluating model performance. ~~We found~~  
597 ~~that the DNN, EGB, GLM, and RF models achieved  $R^2 > 0.8$ , indicating that the model could yield~~  
598 ~~reliable volume estimates in adjacent areas with similar geological and environmental conditions.~~  
599 ~~It is also noted that the EGB, RF, and DNN are designed to efficiently handle large datasets, making~~  
600 ~~them suitable for regional-scale analysis with high scalability. Thus, these models can be scaled to~~  
601 ~~incorporate more data from different geographical areas without significant adjustments,~~  
602 ~~enhancing their applicability in future research (Krizhevsky et al., 2012). Subsequently, the~~  
603 ~~optimized model can aid in disaster risk management by providing timely information for early~~  
604 ~~warning systems. Additionally, the insights gained from the model can inform land-use planning~~  
605 ~~and policy decisions, allowing stakeholders to identify high-risk areas and implement mitigation~~  
606 ~~strategies effectively. By integrating the model into existing monitoring frameworks, agencies can~~

서식 지정함: 글꼴 색: 자동

서식 있음: 금칙 처리 안 함, 단어 잘림 방지, 문장 부호  
끌어 맞추지 않음

서식 지정함: 글꼴 색: 자동

서식 지정함: 글꼴 색: 자동

서식 지정함: 글꼴 색: 자동

서식 지정함: 글꼴 색: 자동

서식 지정함: 글꼴 색: 자동

서식 지정함: 글꼴 색: 자동

서식 지정함: 글꼴 색: 자동

607 ~~enhance their response capabilities and better allocate resources during heavy rainfall~~  
608 ~~events.~~ prediction accuracy. The outcome exhibited that the difference in  $R^2$  on the training and  
609 ~~holdout set of 7.72% for the optimal model (i.e., EGB) highlights that the model can be applied to~~  
610 ~~another region of a similar setting. It was noted that without proper model calibration with the~~  
611 ~~independent data set, it's difficult to determine whether these discrepancies in performance are due~~  
612 ~~to model limitations or data differences in different regions (Huang et al., 2020). Therefore, in~~  
613 ~~future work, we plan to develop an independent database based on collecting the extensive recent~~  
614 ~~landslide geometry at different parts of the Korean Peninsula to improve the models further by~~  
615 ~~calibrating region-specific parameters to ensure the transferability of the model to other regions.~~

서식 지정함: 글꼴 색: 자동

616 The major limitation of this study is that the analysis is solely focused on shallow-seated  
617 landslides, specifically translational slope failures with volumes below 13,000m<sup>3</sup>. Thus, the  
618 analysis may not fully capture the variability in landslide characteristics across different  
619 geomorphological and geological contexts. Deep-seated landslides, for instance, often exhibit  
620 distinct failure mechanisms, material compositions, and depositional patterns that influence their  
621 volumetric characteristics, which were not considered in this investigation. Similarly, debris flows,  
622 known for their unique channelization and entrainment behaviors, were not included, potentially  
623 limiting the applicability of the optimized models to other landslide types. Further, this study was  
624 also performed using point-based landslide inventory data, which may not capture all variability  
625 of influencing factors and their exact state. The incorporation of high-resolution data from remote  
626 sensing and other sources may also improve the efficiency of the predictions. These limitations  
627 may impact the broader applicability of the proposed model; however, future studies will aim to  
628 address this by conducting separate analyses for deep-seated landslides and debris flows, allowing  
629 for a more comprehensive understanding of landslide volume predictions across diverse landslide  
630 types and geomorphological settings.

631

632

## 633 **6. Conclusions**

서식 지정함: 글꼴 색: 자동

634 In this paper, the aim was to construct a data-driven model that predicts the volume of landslides  
635 due to rainfall. To this, nine different classical regression models and machine learning algorithms  
636 were tested on South Korean landslide data set containing features of landslides that occurred  
637 between 2011 and 2012. Among the tested models, ~~extreme gradient boosting (the EGB) model~~

서식 있음: 금칙 처리 안 함, 단어 잘림 방지, 문장 부호  
끌어 맞추지 않음

서식 지정함: 글꼴 색: 자동

서식 지정함: 글꼴 색: 자동

638 produced the most accurate prediction. This is proven by the evaluation of the difference between  
639 actual and predicted values, such as  $R^2= 88.41\%$  and  $MAE=146.6120m^3$  on the testholdout set.  
640 The analysis of feature variables in the contribution to the prediction of the model revealed that  
641 the slope length was the most influencing predictor. The EGB model can be a promising tool for  
642 the prediction of the volume of landslides due to its high predictive performance. The model can  
643 be customized in different environmental settings. The model can be applied to estimate the  
644 expected volume of landslides based on forecasted rainfall once the model is well-adjusted to fit  
645 the geomorphological and environmental settings of the region of interest after re-training on the  
646 regional historical data to include regional variability. Therefore, this model can be a good tool for  
647 planning for resilience and infrastructure pre-construction risk assessment to ensure the new  
648 infrastructure is placed in stable regions free from severe landslides.

서식 지정함: 글꼴 색: 자동

#### 650 Acknowledgments

651 This research was supported by the Korean government (MSIT) (2021R1C1C2003316) and Basic  
652 Science Research Program through the National Research Foundation of Korea (NRF) funded by  
653 Ministry of Education (2021R1A6A1A03044326).

654 The authors highly appreciate both anonymous reviewers and editor for their constructive  
655 suggestions that helped us improve the preprint version.

서식 지정함: 글꼴 색: 자동

서식 지정함: 글꼴 색: 자동

서식 있음: 금칙 처리 안 함, 문장 부호 끌어 맞추지  
않음, 한글과 영어 간격을 자동으로 조절하지 않음,  
한글과 숫자 간격을 자동으로 조절하지 않음

서식 있음: 금칙 처리 안 함, 단어 잘림 방지, 문장 부호  
끌어 맞추지 않음

#### 657 Reference

658 Alcantara, A. L., and Ahn, K. H. (2020). Probability distribution and characterization of daily  
659 precipitation related to tropical cyclones over the Korean Peninsula. *Water*, 12(4), 1214.  
660 <https://doi.org/10.3390/w12041214>

서식 지정함: 글꼴 색: 자동

661 [Aleántara Ayala, I. \(2021\). Integrated landslide disaster risk management \(ILDRIIM\): the challenge  
662 to avoid the construction of new disaster risk. \*Environmental Hazards\*, 20\(3\), 323-344.](#)

663 [Aleántara Ayala, I., & Alcántara-Ayala, I., and Sassa, K. \(2023\). Landslide risk management: from  
664 hazard to disaster risk reduction. \*Landslides\*, 20\(10\), 2031-2037.  
665 <https://doi.org/10.1007/s10346-023-02140-5>](#)

서식 지정함: 글꼴 색: 자동, 영어(미국)

서식 지정함: 글꼴 색: 자동

서식 지정함: 글꼴 색: 자동

666 [Amatya, S. C. \(2016\). Landslide disaster management in Nepal: a near future perspective. \*Nepal-  
667 Japan Friendship Association of Water Induced Disaster \(NFAD\), Japan Department of  
668 Water Induced Disaster Management \(DWIDM\).\*](#)

669 [Amesoder, C., Hartig, F., and Pichler, M. \(2023\). cito: An R package for training neural networks  
670 using torch. arXiv e-prints, arXiv-2303. <https://doi.org/10.1111/ecog.07143>](#)

서식 지정함: 글꼴 색: 자동

서식 지정함: 글꼴 색: 자동

671 Armstrong, J. S. (2001). Combining forecasts (pp. 417-439). Springer US.  
672 [https://doi.org/10.1007/978-0-306-47630-3\\_19](https://doi.org/10.1007/978-0-306-47630-3_19)

673 Asada, H., & Minagawa, T. (2023). Impact of vegetation differences on shallow landslides: a  
674 case study in Aso, Japan. *Water*, 15(18), 3193. <https://doi.org/10.3390/w15183193>

675 ~~Barik, M. G., Adam, J. C., Barber, M. E., & Muhunthan, B. (2017). Improved landslide~~  
676 ~~susceptibility prediction for sustainable forest management in an altered climate.~~  
677 ~~*Engineering geology*, 230, 104-117.~~

678 Bernardie, S., Desramaut, N., Malet, J.-P., Gourlay, M., and Grandjean, G. (2014). Prediction of  
679 changes in landslide rates induced by rainfall. *Landslides*, 12(3), 481-494.  
680 [doi:10.1007/s10346-014-0495-8](https://doi.org/10.1007/s10346-014-0495-8)<https://doi.org/10.1007/s10346-014-0495-8>

681 Bonamutial, M., and Prasetyo, S. Y. (2023, August). Exploring the Impact of Feature Data  
682 Normalization and Standardization on Regression Models for Smartphone Price  
683 Prediction. In 2023 International Conference on Information Management and  
684 Technology (ICIMTech) (pp. 294-298). IEEE.  
685 <https://doi.org/10.1109/ICIMTech59029.2023.10277860>

686 Borup, D., Christensen, B. J., Mühlbach, N. S., and Nielsen, M. S. (2023). Targeting predictors in  
687 random forest regression. *International Journal of Forecasting*, 39(2), 841-868.  
688 <https://doi.org/10.1016/j.ijforecast.2022.02.010>

689 Breiman, L. (2001). Random forests. *Machine learning*, 45, 5-32. [https://doi.org/](https://doi.org/10.1023/A:1010933404324)  
690 [10.1023/A:1010933404324](https://doi.org/10.1023/A:1010933404324)

691 Breiman, L. (2017). Classification and regression trees. Routledge. [https://doi.org](https://doi.org/10.1201/9781315139470)  
692 [/10.1201/9781315139470](https://doi.org/10.1201/9781315139470)

693 Caine, N. (1980). The rainfall intensity-duration control of shallow landslides and debris flows.  
694 *Geografiska annaler: series A, physical geography*, 62(1-2), 23-27.  
695 <https://doi.org/10.1080/04353676.1980.11879996>

696 Cellek, S. (2021). The effect of aspect on landslide and its relationship with other parameters. In  
697 Landslides. IntechOpen.

698 Chang, K. T., and Chiang, S. H. (2009). An integrated model for predicting rainfall-induced  
699 landslides. *Geomorphology*, 105(3-4), 366-373. [https://doi.org/10.1016/](https://doi.org/10.1016/j.geomorph.2008.10.012)  
700 [j.geomorph.2008.10.012](https://doi.org/10.1016/j.geomorph.2008.10.012)

701 Chang, K. T., Chiang, S. H., and Lei, F. (2008). Analysing the relationship between typhoon-  
702 triggered landslides and critical rainfall conditions. *Earth Surface Processes and*  
703 *Landforms: The Journal of the British Geomorphological Research Group*, 33(8), 1261-  
704 1271. <https://doi.org/10.1002/esp.1611>

705 Chatra, A. S., Dodagoudar, G. R., & Maji, V. B. (2019). Numerical modelling of rainfall effects  
706 on the stability of soil slopes. *International Journal of Geotechnical Engineering*.  
707 <https://doi.org/10.1080/19386362.2017.1359912>

708 Chen T., He T., Benesty M., Khotilovich V., Tang Y., Cho H., Chen K., Mitchell R., Cano  
709 I., Zhou T., Li M., Xie J., Lin M., Geng Y., Li Y., and Yuan J. (2022). xgboost:

서식 지정함: 글꼴 색: 자동

서식 지정함: 글꼴 색: 자동

서식 지정함: 글꼴 색: 자동

서식 지정함

서식 지정함: 글꼴 색: 자동

서식 지정함: 글꼴 색: 자동

서식 지정함: 글꼴 색: 자동

서식 지정함: 글꼴 색: 자동

서식 지정함: 글꼴 색: 자동

서식 지정함: 글꼴 색: 자동

서식 지정함: 글꼴 색: 자동

서식 지정함: 글꼴 색: 자동

서식 지정함: 글꼴 색: 자동

서식 지정함: 글꼴 색: 자동

서식 지정함: 글꼴 색: 자동

서식 지정함: 글꼴 색: 자동

서식 지정함

710 Extreme Gradient Boosting. R package version 1.6.0.1, <[https://CRAN.R-](https://CRAN.R-project.org/package=xgboost)

711 [project.org/package=xgboost](https://CRAN.R-project.org/package=xgboost)>>. [Accessed 2025-01-25]

712 Chen, C. W., Oguchi, T., Hayakawa, Y. S., Saito, H., and Chen, H. (2017). Relationship between

713 landslide size and rainfall conditions in Taiwan. *Landslides*, 14, 1235-1240.

714 <https://doi.org/10.1007/s10346-016-0790-7>.

715 Chen, L., Guo, Z., Yin, K., Shrestha, D. P., & Jin, S. (2019). The influence of land use and land

716 cover change on landslide susceptibility: a case study in Zhushan Town, Xuan'en County

717 (Hubei, China). *Natural Hazards and Earth System Sciences*, 19(10), 2207-2228. <https://doi.org/10.5194/nhess-19-2207-2019>.

718 Chen, T., & Guestrin, C. (2016). Xgboost: A scalable tree boosting system. In Proceedings of

719 the 22nd acm sigkdd international conference on knowledge discovery and data mining

720 (pp. 785-794).

721 [doi:10.1145/2939672.2939785](https://doi.org/10.1145/2939672.2939785)

722 <https://doi.org/10.1145/2939672.2939785>.

723 Chen, T., He, T., Benesty, M., Khotilovich, V., Tang, Y., Cho, H., ... and Zhou, T. (2015b). Xgboost:

724 extreme gradient boosting. *R package version 0.4-2*, 1(4), 1(4).

725 Chen, X., Zhang, L., Zhang, L., Zhou, Y., Ye, G., and Guo, N. (2021). Modelling rainfall-induced

726 landslides from initiation of instability to post-failure. *Computers and Geotechnics*, 129,

727 [103877](https://doi.org/10.1016/j.compgeo.2020.103877). <https://doi.org/10.1016/j.compgeo.2020.103877>

728 Chen, Z., Luo, R., Huang, Z., Tu, W., Chen, J., Li, W., ... and Ai, Y. (2015a). Effects of different

729 backfill soils on artificial soil quality for cut slope revegetation: Soil structure, soil

730 erosion, moisture retention and soil C stock. *Ecological Engineering*, 83, 5-

731 12. <https://doi.org/10.1016/j.ecoleng.2015.05.048>.

732 ~~Chen, T., He, T., Benesty, M., Khotilovich, V., Tang, Y., Cho, H., ... and Zhou, T. (2015b). Xgboost:~~

733 ~~extreme gradient boosting. R package version 0.4-2~~, 1(4), 1(4).

734 ~~Chen, X., Zhang, L., Zhang, L., Zhou, Y., Ye, G., & Guo, N. (2021). Modelling rainfall induced~~

735 ~~landslides from initiation of instability to post-failure. Computers and geotechnics, 129,~~

736 ~~103877.~~

737 Cheung, R. W. (2021). Landslide risk management in Hong Kong. *Landslides*, 18(10), 3457-3473.

738 <https://doi.org/10.1007/s10346-020-01587-0>.

739 Chicco, D., Warrens, M. J., & Jurman, G. (2021). The coefficient of determination R-squared

740 is more informative than SMAPE, MAE, MAPE, MSE and RMSE in regression analysis

741 evaluation. *PeerJ computer science*, 7, e623. *PeerJ Computer Science*, 7, e623.

742 <https://doi.org/10.7717/peerj-cs.623>.

743 Chowdhury, M. Z. I., Leung, A. A., Walker, R. L., Sikdar, K. C., O'Beirne, M., Quan, H., and

744 Turin, T. C. (2023). A comparison of machine learning algorithms and traditional

745 regression-based statistical modeling for predicting hypertension incidence in a Canadian

746 population. *Scientific Reports*, 13(1), 13. <https://doi.org/10.1038/s41598-022-27264-x>.

747 Chung, C. J. F., and Fabbri, A. G. (2003). Validation of spatial prediction models for landslide

748 hazard mapping. *Natural Hazards*, 30, 451-472. [https://doi.org/10.1023/](https://doi.org/10.1023/B:NHAZ.0000007172.62651.2b)

749 [B:NHAZ.0000007172.62651.2b](https://doi.org/10.1023/B:NHAZ.0000007172.62651.2b)

서식 지정함: 글꼴 색: 자동, 프랑스어(프랑스)

서식 지정함: 글꼴 색: 자동, 프랑스어(프랑스)

서식 지정함: 글꼴 색: 자동

서식 지정함: 글꼴 색: 자동

서식 지정함: 글꼴 색: 자동

서식 지정함: 글꼴 색: 자동

서식 지정함: 글꼴 색: 자동

서식 지정함: 글꼴 색: 자동

서식 지정함: 글꼴 색: 자동

서식 지정함: 글꼴 색: 자동, 프랑스어(프랑스)

서식 지정함: 글꼴 색: 자동

서식 지정함: 글꼴 색: 자동, 영어(미국)

서식 지정함: 글꼴 색: 자동

서식 지정함: 글꼴 색: 자동, 프랑스어(프랑스)

서식 지정함: 글꼴 색: 자동

서식 있음: 탭: 4.5 글자(없음)

서식 지정함: 글꼴 색: 자동

서식 지정함: 글꼴 색: 자동

서식 지정함: 글꼴 색: 자동, 영어(미국)

서식 지정함: 글꼴 색: 자동

서식 지정함: 글꼴 색: 자동

서식 지정함: 글꼴 색: 자동

서식 지정함: 글꼴 색: 자동

서식 지정함: 글꼴 색: 자동

서식 지정함: 글꼴 색: 자동

750 Cohen, D., & Schwarz, M. (2017). Tree-root control of shallow landslides. *Earth Surface*  
751 *Dynamics*, 5(3), 451-477. <https://doi.org/10.5194/esurf-5-451-2017>.

752 Conte, E., Pugliese, L., and Troneone, A. (2022). A simple method for predicting rainfall-induced  
753 shallow landslides. *Journal of Geotechnical and Geoenvironmental Engineering*,  
754 148(10), 04022079.

755 Culler, E. S., Livneh, B., Rajagopalan, B., & Tiampo, K. F. (2021). A data-driven evaluation of  
756 post-fire landslide susceptibility. *Natural Hazards and Earth System Sciences*  
757 *Discussions*, 2021, 1-24. <https://doi.org/10.5194/nhess-23-1631-2023>.

758 Dahal, B. K., and Dahal, R. K. (2017). Landslide hazard map: tool for optimization of low-cost  
759 mitigation. *Geoenvironmental Disasters*, 4, 1-9. <https://doi.org/10.1186/s40677-017-0071-3>

760 Dai, F. C., & Lee, C. F. (2001). Frequency-volume relation and prediction of rainfall-induced  
761 landslides. *Engineering geology*, 59(3-4), 253-266.  
762 [https://doi.org/10.1016/S0013-7952\(00\)00077-6](https://doi.org/10.1016/S0013-7952(00)00077-6).

763 Dai, F. C., Lee, C. F., & Ngai, Y. Y. (2002). Landslide risk assessment and management: an  
764 overview. *Engineering geology*, 64(1), 65-87.

765 Dai, K., Xu, Q., Li, Z., Tomás, R., Fan, X., Dong, X., ... and Ran, P. (2019). Post-disaster  
766 assessment of 2017 catastrophic Xinmo landslide (China) by spaceborne SAR  
767 interferometry. *Landslides*, 16, 1189-1199.

768 Darlington, R. B. (1990). *Regression and linear models*. McGraw-Hill College.

769 Dikshit, A., Satyam, N., & Pradhan, B., 2019. Estimation of rainfall-induced landslides using the  
770 TRIGRS model. *Earth Systems and Environment*, 3, 575-584.

771 Dinno, A. (2015). Nonparametric pairwise multiple comparisons in independent groups using  
772 Dunn's test. *The Stata Journal*, 15(1), 292-300. <https://doi.org/10.1177/1536867X1501500117>.

773 Dismuke, C., and Lindrooth, R. (2006). Ordinary least squares. *Methods and designs for outcomes*  
774 *research*, 93(1), 93-104.

775 Dobson, A. J., and Barnett, A. G. (2018). *An introduction to generalized linear models*. CRC press.  
776 <https://doi.org/10.1201/9781315182780>

777 Donnarumma, A., Revellino, P., Grelle, G., and Guadagno, F. M. (2013). Slope angle as indicator  
778 parameter of landslide susceptibility in a geologically complex area. *Landslide Science*  
779 *and Practice: Volume 1: Landslide Inventory and Susceptibility and Hazard Zoning*, 425-  
780 433. [https://doi.org/10.1007/978-3-642-31325-7\\_56](https://doi.org/10.1007/978-3-642-31325-7_56).

781 Duc, D. M. (2013). Rainfall-triggered large landslides on 15 December 2005 in Van Canh district,  
782 Binh Dinh province, Vietnam. *Landslides*, 10(2), 219-230. <https://doi.org/10.1007/s10346-012-0362-4>.

783 Dudley, R. (2023). The Shapiro-Wilk test for normality. Available at  
784 <https://math.mit.edu/~rmd/46512/shapiro.pdf> [Accessed 2025-01-25].

785 Evans, S. G., Mugnozza, G. S., Strom, A., and Hermanns, R. L. (Eds.). (2007). *Landslides from*  
786 *massive rock slope failure* (Vol. 49). Springer Science and Business Media.

서식 지정함: 글꼴 색: 자동

서식 지정함: 글꼴 색: 자동

서식 지정함: 글꼴 색: 자동

서식 지정함: 글꼴 색: 자동

서식 지정함: 글꼴 색: 자동

서식 있음: 탭: 4.5 글자(없음)

서식 지정함: 하이퍼링크, 글꼴: +본문(Calibri), 11 pt, 글꼴 색: 자동

서식 지정함: 글꼴 색: 자동

서식 지정함: 글꼴 색: 자동

서식 지정함: 글꼴 색: 자동

서식 지정함: 글꼴 색: 자동

서식 지정함: 글꼴 색: 자동

서식 지정함: 글꼴 색: 자동

서식 지정함: 글꼴 색: 자동

서식 지정함: 글꼴 색: 자동

서식 지정함: 글꼴 색: 자동

서식 지정함: 글꼴 색: 자동

서식 지정함: 글꼴 색: 자동

서식 지정함: 글꼴 색: 자동

서식 지정함: 글꼴 색: 자동

서식 지정함: 글꼴 색: 자동

서식 지정함: 하이퍼링크, 글꼴: +본문(Calibri), 11 pt, 글꼴 색: 자동

서식 지정함: 글꼴 색: 자동

서식 지정함: 글꼴 색: 자동

서식 지정함: 글꼴 색: 자동

서식 있음: 탭: 4.5 글자(없음)

서식 지정함: 글꼴 색: 자동



790 Fan, X., Xu, Q., Liu, J., Subramanian, S. S., He, C., Zhu, X., & Zhou, L. (2019). Successful early  
 791 warning and emergency response of a disastrous rockslide in Guizhou province, China.  
 792 *Landslides*, 16, 2445-2457.

793 Fan, X., Xu, Q., Searingi, G., Dai, L., Li, W., Dong, X., ... & Havenith, H. B. (2017). Failure  
 794 mechanism and kinematics of the deadly June 24th 2017 Xinmo landslide, Maoxian,  
 795 Sichuan, China. *Landslides*, 14, 2129-2146. <https://doi.org/10.1007/s10346-017-0907-7>

796 Friedman, J. H., Hastie, T., & Tibshirani, R. (2010). Regularization paths for generalized linear  
 797 models via coordinate descent. *Journal of statistical software*, 33, 1-22. (misquoted in the  
 798 paper as Jerome 2012). Available at <https://pmc.ncbi.nlm.nih.gov/articles/PMC2929880/>.

799 Gariano, S. L., Rianna, G., Petrucci, O., and Guzzetti, F. (2017). Assessing future changes in the  
 800 occurrence of rainfall-induced landslides at a regional scale. *Science of the total  
 801 environment*, 596, 417-426.  
 802 <https://doi.org/10.1016/j.scitotenv.2017.03.103>

803 Gelman, A. (2007). Data analysis using regression and multilevel/hierarchical models. Cambridge  
 804 University Press.

805 Glade, T., Anderson, M. G., and Crozier, M. J. (2005). *Landslide hazard and risk (Vol. 807)*. John  
 806 Wiley & Sons. <https://doi.org/10.1002/9780470012659>

807 Gong, Q., Wang, J., Zhou, P., and Guo, M. (2021). A regional landslide stability analysis method  
 808 under the combined impact of rainfall and vegetation roots in south China. *Advances in  
 809 Civil Engineering*, 2021, 1-12. <https://doi.org/10.1155/2021/5512281>.

810 Gonzalez-Ollauri, A., and Mickovski, S. B. (2017). Hydrological effect of vegetation against  
 811 rainfall-induced landslides. *Journal of Hydrology*, 549, 374-387.  
 812 <https://doi.org/10.1016/j.jhydrol.2017.04.014>

813 Greenwood, J. R., Norris, J. E., & Wint, J. (2004). Assessing the contribution of vegetation to  
 814 slope stability. *Proceedings of the Institution of Civil Engineers-Geotechnical  
 815 Engineering*, 157(4), 199-207. <https://doi.org/10.1680/geng.2004.157.4.199>

816 Gutierrez-Martin, A. (2020). A GIS-physically-based emergency methodology for predicting  
 817 rainfall-induced shallow landslide zonation. *Geomorphology*, 359, 107121.  
 818 <https://doi.org/10.1016/j.geomorph.2020.107121>

819 Guzzetti, F., Peruccacci, S., Rossi, M., & Stark, C. P. (2008). The rainfall intensity-duration  
 820 control of shallow landslides and debris flows: an update. *Landslides*, 5, 3-17.  
 821 <https://doi.org/10.1007/s10346-007-0112-1>

822 Ha, K. M. (2022). predicting typhoon tracks around Korea. *Natural Hazards*, 113(2), 1385-1390.  
 823 <https://doi.org/10.1007/s11069-022-05335-6>

824 Hastie, T. (2009). The elements of statistical learning: data mining, inference, and prediction. 2nd  
 825 edition. <https://doi.org/10.1111/j.1541-0420.2010.01516.x>

826 Highland, L. and Bobrowsky, P. (2008). *The Landslide Handbook: A Guide to Understanding  
 827 Landslides*, United States Geological Survey, Reston, VA, Circular 1325,  
 828 <https://pubs.usgs.gov/circ/1325/> (last access: 6 March 2023). Available at  
 829 <https://pubs.usgs.gov/circ/1325/> [ Accessed: 2025-01-25]

서식 지정함: 글꼴 색: 자동, 영어(미국)

서식 지정함: 글꼴 색: 자동, 영어(미국)

서식 지정함: 글꼴 색: 자동

서식 지정함: 글꼴 색: 자동

서식 지정함: 글꼴 색: 자동

서식 있음: 탭: 4.5 글자(없음)

서식 지정함: 글꼴 색: 자동

서식 지정함: 글꼴 색: 자동

서식 지정함: 글꼴 색: 자동

서식 지정함: 글꼴 색: 자동, 영어(미국)

서식 지정함: 글꼴 색: 자동

서식 지정함: 글꼴 색: 자동

서식 지정함: 글꼴 색: 자동

서식 지정함: 글꼴 색: 자동

서식 있음: 탭: 4.5 글자(없음)

서식 지정함: 글꼴 색: 자동

서식 지정함: 글꼴 색: 자동

서식 지정함: 글꼴 색: 자동

서식 지정함: 글꼴 색: 자동

서식 지정함: 글꼴 색: 자동

서식 지정함: 글꼴 색: 자동

서식 있음: 탭: 4.5 글자(없음)

서식 지정함: 글꼴 색: 자동



830 Holcombe, E. A., Beesley, M. E., Vardanega, P. J., & Sorbie, R. (2016, ~~March~~). Urbanisation  
831 and landslides: hazard drivers and better practices. In Proceedings of the Institution of  
832 Civil Engineers-Civil Engineering (Vol. 169, ~~No. (3)~~), pp. 137-144). Thomas Telford Ltd.  
833 <https://doi.org/10.1680/jcien.15.00044>

834 Hovius, N., Stark, C. P., & Allen, P. A. (1997). Sediment flux from a mountain belt derived by  
835 landslide mapping. *Geology*, 25(3), 231-234. [https://doi.org/10.1130/0091-7613\(1997\)025<0231:SFFAMB>2.3.CO;2](https://doi.org/10.1130/0091-7613(1997)025<0231:SFFAMB>2.3.CO;2)

837 [Huang, J., Hales, T. C., Huang, R., Ju, N., Li, Q., and Huang, Y. \(2020\). A hybrid machine-learning model to estimate potential debris-flow volumes. \*Geomorphology\*, 367, 107333. <https://doi.org/10.1016/j.geomorph.2020.107333>](https://doi.org/10.1016/j.geomorph.2020.107333)

840 Hyde, K. D., Riley, K., & Stoof, C. (2016). Uncertainties in predicting debris flow hazards  
841 following wildfire. *Natural Hazards*. <https://doi.org/10.1002/9781119028116.ch19>

842 Hyndman, R. J., & Koehler, A. B. (2006). Another look at measures of forecast accuracy.  
843 *International Journal of Forecasting*, 22(4), 679-688.  
844 <https://doi.org/10.1016/j.ijforecast.2006.03.001>

846 Hyun, Y. K., Kar, S. K., Ha, K. J., & Lee, J. H. (2010). Diurnal and spatial variabilities of  
847 monsoonal CG lightning and precipitation and their association with the synoptic weather  
848 conditions over South Korea. *Theoretical and applied climatology*~~Applied Climatology~~,  
849 102, 43-60. <https://doi.org/10.1007/s00704-009-0235-5>

850 Intrieri, E., Carlà, T., and Gigli, G. (2019). Forecasting the time of failure of landslides at slope-  
851 scale: A literature review. *Earth-science reviews*, 193, 333-349.  
852 <https://doi.org/10.1016/j.earscirev.2019.03.019>

853 ~~Islam, M. A., Islam, M. S., & Islam, T. (2017, September). Landslides in Chittagong hill tracts and possible measures. In Proceedings of the international conference on disaster risk mitigation, Dhaka, Bangladesh (Vol. 23).~~

856 ~~Jaboyedoff, M., Choffet, M., Derron, M. H., Horton, P., Loye, A., Longchamp, C., Mazotti, B., Michoud, C., and Pedrazzini, A. (2012). Preliminary slope mass movement susceptibility mapping using DEM and LiDAR DEM. In Terrestrial mass movements: Detection, modelling, early warning and mitigation using geoinformation technology, 109-170. Springer, Berlin Heidelberg. [https://doi.org/10.1007/978-3-642-25495-6\\_5](https://doi.org/10.1007/978-3-642-25495-6_5)~~

861 Jin, H. G., Lee, H., & Baik, J. J. (2022). Characteristics and possible mechanisms of diurnal  
862 variation of summertime precipitation in South Korea. *Theoretical and Applied*  
863 *Climatology*, 148(1), 551-568. <https://doi.org/10.1007/s00704-022-03965-1>

864 Ju, L. Y., Zhang, L. M., and Xiao, T. (2023). Power laws for accurate determination of landslide  
865 volume based on high-resolution LiDAR data. *Engineering Geology*, 312, 106935.  
866 <https://doi.org/10.1016/j.enggeo.2022.106935>

867 Jung, M. J., Jeong, Y. J., Shin, W. J., & Cheong, A. C. S. (2024). Isotopic distribution of  
868 bioavailable Sr, Nd, and Pb in Chungcheongbuk-do Province, Korea. *Journal of*

서식 지정함: 글꼴 색: 자동

서식 지정함: 글꼴 색: 자동

서식 지정함: 글꼴 색: 자동

서식 지정함: 글꼴 색: 자동

서식 지정함: 글꼴 색: 자동

서식 지정함: 글꼴 색: 자동

서식 지정함: 글꼴 색: 자동

서식 지정함: 글꼴 색: 자동

서식 지정함: 글꼴 색: 자동

서식 지정함: 글꼴 색: 자동

서식 지정함: 글꼴 색: 자동

서식 지정함: 글꼴 색: 자동

서식 지정함: 글꼴 색: 자동

서식 지정함: 글꼴 색: 자동

서식 지정함: 글꼴 색: 자동

서식 지정함: 글꼴 색: 자동

서식 지정함: 글꼴 색: 자동

서식 지정함: 글꼴 색: 자동

서식 지정함: 글꼴 색: 자동

서식 지정함: 글꼴 색: 자동

서식 지정함: 글꼴 색: 자동

서식 지정함: 글꼴 색: 자동

서식 지정함: 글꼴 색: 자동

서식 있음: 탭: 4.5 글자, 왼쪽

서식 지정함: 글꼴 색: 자동

서식 지정함: 글꼴 색: 자동

869 Analytical Science and Technology, 15(1), 46. [https://doi.org/10.1186/s40543-024-](https://doi.org/10.1186/s40543-024-00460-2)  
870 [00460-2](https://doi.org/10.1186/s40543-024-00460-2)

871 Jung, Y., Shin, J. Y., Ahn, H., and Heo, J. H. (2017). The spatial and temporal structure of extreme  
872 rainfall trends in South Korea. *Water*, 9(10), 809. <https://doi.org/10.3390/w9100809>

873 Kafle, L., Xu, W. J., Zeng, S. Y., & Nagel, T. (2022). A numerical investigation of slope stability  
874 influenced by the combined effects of reservoir water level fluctuations and precipitation:  
875 A case study of the Bianjiazhai landslide in China. *Engineering Geology*, 297, 106508.  
876 <https://doi.org/10.1016/j.enggeo.2021.106508>

877 Kang, M. W., Yibeltal, M., Kim, Y. H., Oh, S. J., Lee, J. C., Kwon, E. E., & Lee, S. S. (2022).  
878 Enhancement of soil physical properties and soil water retention with biochar-based soil  
879 amendments. *Science of the total environment* *Total Environment*, 836, 155746.  
880 <https://doi.org/10.1016/j.scitotenv.2022.155746>

881 Keefer, R. F. (2000). *Handbook of soils for landscape architects*. Oxford University Press.

882 Khan, M. A., Basharat, M., Riaz, M. T., Sarfraz, Y., Farooq, M., Khan, A. Y., & Pham, Q. B.,  
883 Ahmed, K. S., and Shahzad, A. (2021). An integrated geotechnical and geophysical  
884 investigation of a catastrophic landslide in the Northeast Himalayas of Pakistan.  
885 *Geological Journal*, 56(9), 4760-4778. <https://doi.org/10.1002/gj.4209>

886 Khan, Y. A., Latch, H., Baten, M. A., and Kamil, A. A. (2012). Critical antecedent rainfall  
887 conditions for shallow landslides in Chittagong City of Bangladesh. *Environmental Earth*  
888 *Sciences*, 67, 97-106. <https://doi.org/10.1007/s12665-011-1483-0>

889 Kim, D. E., Seong, Y. B., Weber, J., & Yu, B. Y. (2020). Unsteady migration of Taebaek  
890 Mountain drainage divide, Cenozoic extensional basin margin, Korean Peninsula.  
891 *Geomorphology*, 352, 107012. <https://doi.org/10.1016/j.geomorph.2019.107012>

892 Kim, H. G., & Park, C. Y. (2021). Landslide susceptibility analysis of photovoltaic power  
893 stations in Gangwon-do, Republic of Korea. *Geomatics, Natural Hazards and Risk*, 12(1),  
894 2328-2351. <https://doi.org/10.1080/19475705.2021.1950219>

895 Kim, J., Lee, K., Jeong, S., & Kim, G. (2014). GIS-based prediction method of landslide  
896 susceptibility using a rainfall infiltration-groundwater flow model. *Engineering*  
897 *geology* *Geology*, 182, 63-78. <https://doi.org/10.1016/j.enggeo.2014.09.001>

898 Kim, M. S., Onda, Y., Kim, J. K., & Kim, S. W. (2015). Effect of topography and soil  
899 parameterisation representing soil thicknesses on shallow landslide modelling.  
900 *Quaternary International*, 384, 91-106. <https://doi.org/10.1016/j.quaint.2015.03.057>

901 Kim, S. W., Chun, K. W., Kim, M., Catani, F., Choi, B., and Seo, J. I. (2021). Effect of antecedent  
902 rainfall conditions and their variations on shallow landslide-triggering rainfall thresholds  
903 in South Korea. *Landslides*, 18, 569-582. <https://doi.org/10.1007/s10346-020-01505-4>

904 Kitutu, M. G., Muwanga, A., Poesen, J., and Deckers, J. A. (2009). Influence of soil properties on  
905 landslide occurrences in Bududa district, Eastern Uganda. *African journal of*  
906 *agricultural research* *Agricultural Research*, 4(7), 611-620. Available at  
907 <https://lirias.kuleuven.be/retrieve/78489> [Accessed 2025-01-25].

서식 지정함: 글꼴 색: 자동

서식 지정함: 글꼴 색: 자동

서식 지정함: 글꼴 색: 자동

서식 지정함: 글꼴 색: 자동

서식 지정함: 글꼴 색: 자동

서식 있음: 탭: 4.5 글자, 왼쪽

서식 지정함: 글꼴 색: 자동

서식 지정함: 글꼴 색: 자동

서식 지정함: 글꼴 색: 자동

서식 지정함: 글꼴 색: 자동

서식 있음: 탭: 4.5 글자, 왼쪽

서식 지정함: 글꼴 색: 자동

서식 지정함: 글꼴 색: 자동

서식 지정함: 글꼴 색: 자동

서식 지정함: 글꼴 색: 자동

서식 지정함: 글꼴 색: 자동

서식 지정함: 글꼴 색: 자동

서식 지정함: 글꼴 색: 자동

서식 지정함: 글꼴 색: 자동

서식 지정함: 글꼴 색: 자동

서식 지정함: 글꼴 색: 자동

서식 지정함: 글꼴 색: 자동

서식 지정함: 글꼴 색: 자동

서식 지정함: 글꼴 색: 자동

서식 지정함: 글꼴 색: 자동

908 [Klimeš, J., Stemberk, J., Blahut, J., Krejčí, V., Krejčí, O., Hartvich, F., & Kyel, P. \(2017\). Challenges for landslide hazard and risk management in ‘low risk’ regions, Czech Republic—landslide occurrences and related costs \(IPL project no. 197\). \*Landslides\*, 14, 771–780](#)

909

910

911

912 [Korup, O. \(2004\). Geomorphometric characteristics of New Zealand landslide dams. \*Engineering Geology\*, 73\(1-2\), 13-35. <https://doi.org/10.1016/j.enggeo.2003.11.003>](#)

913

914 [Korup, O., Clague, J. J., Hermanns, R. L., Hewitt, K., Strom, A. L., and Weidinger, J. T. \(2007\). Giant landslides, topography, and erosion. \*Earth and Planetary Science Letters\*, 261\(3-4\), 578-589. <https://doi.org/10.1016/j.epsl.2007.07.025>](#)

915

916

917 [Kotsakis, C. \(2023\). Ordinary Least Squares. In \*Encyclopedia of Mathematical Geosciences\* \(pp. 1032-1038\). Cham: Springer International Publishing. \[https://doi.org/10.1007/978-3-030-85040-1\\\_237\]\(https://doi.org/10.1007/978-3-030-85040-1\_237\)](#)

918

919

920 [Kramer, O., and Kramer, O. \(2013\). K-nearest neighbors. Dimensionality reduction with unsupervised nearest neighbors, 13-23. \[https://doi.org/10.1007/978-3-642-38652-7\\\_2\]\(https://doi.org/10.1007/978-3-642-38652-7\_2\)](#)

921

922 [Krizhevsky, A., Sutskever, I., & Hinton, G. E. \(2012\). Imagenet classification with deep convolutional neural networks. \*Advances in neural information processing systems\*, 25. Available at \[https://proceedings.neurips.cc/paper\\\_files/paper/2012/file/c399862d3b9d6b76c8436e924a68c45b-Paper.pdf\]\(https://proceedings.neurips.cc/paper\_files/paper/2012/file/c399862d3b9d6b76c8436e924a68c45b-Paper.pdf\) \[Accessed 2025-01-25\].](#)

923

924

925

926

927 [Kuhn, M. \(2022\). caret: Classification and Regression Training . R package version 6.0-92, <Available at <https://CRAN.R-project.org/package=caret>> \[Accessed 2025-01-25\]](#)

928

929 [Kunz, M., & Kottmeier, C. \(2006\). Orographic enhancement of precipitation over low mountain ranges. Part II: Simulations of heavy precipitation events over southwest Germany. \*Journal of applied meteorology and climatology\*, 45\(8\), 1041-1055. <https://doi.org/10.1175/JAM2390.1>](#)

930

931

932

933 [Lacerda, W. A., Palmeira, E. M., Netto, A. L. C., & Ehrlich, M. \(Eds.\). \(2014\). Extreme rainfall induced landslides: an international perspective. Oficina de Textos. ISBN 978-85-7975-150-9.](#)

934

935

936 [Lann, T., Bao, H., Lan, H., Zheng, H., & Yan, C. \(2024\). Hydro-mechanical effects of vegetation on slope stability: A review. \*Science of the Total Environment\*, 171691. <https://doi.org/10.1016/j.scitotenv.2024.171691>](#)

937

938

939 [LeCun, Y., Bengio, Y., and Hinton, G. \(2015\). Deep learning. \*nature\*\*Nature\*, 521\(7553\), 436-444. <https://doi.org/10.1038/nature14539>](#)

940

941 [Lee, D. B., Kim, Y. N., Sonn, Y. K., & Kim, K. H. \(2023\). Comparison of Soil Taxonomy \(2022\) and WRB \(2022\) Systems for classifying Paddy Soils with different drainage grades in South Korea. \*Land\*, 12\(6\), 1204. <https://doi.org/10.3390/land12061204>](#)

942

943

944 [Lee, D. H., Cheon, E., Lim, H. H., Choi, S. K., Kim, Y. T., & Lee, S. R. \(2021\). An artificial neural network model to predict debris-flow volumes caused by extreme rainfall in the central region of South Korea. \*Engineering Geology\*, 281, 105979. <https://doi.org/10.1016/j.enggeo.2020.105979>](#)

945

946

947

- 서식 지정함: 글꼴 색: 자동
- 서식 있음: 탭: 4.5 글자, 왼쪽
- 서식 지정함: 글꼴 색: 자동
- 서식 지정함: 글꼴 색: 자동
- 서식 지정함: 글꼴 색: 자동
- 서식 지정함: 글꼴 색: 자동
- 서식 지정함: 글꼴 색: 자동
- 서식 지정함: 글꼴 색: 자동
- 서식 지정함: 글꼴 색: 자동, 프랑스어(프랑스)
- 서식 지정함: 하이퍼링크, 글꼴: +본문(Calibri), 11 pt, 글꼴 색: 자동, 프랑스어(프랑스)
- 서식 지정함: 글꼴 색: 자동, 프랑스어(프랑스)
- 서식 지정함: 글꼴 색: 자동
- 서식 지정함: 글꼴 색: 자동
- 서식 있음: 탭: 4.5 글자(없음)
- 서식 지정함: 글꼴 색: 자동
- 서식 지정함: 글꼴 색: 자동
- 서식 지정함: 글꼴 색: 자동
- 서식 지정함: 글꼴 색: 자동
- 서식 지정함: 글꼴 색: 자동
- 서식 지정함: 글꼴 색: 자동
- 서식 지정함: 글꼴 색: 자동
- 서식 지정함: 글꼴 색: 자동
- 서식 지정함: 글꼴 색: 자동

948 Lee, D. H., Kim, Y. T., and Lee, S. R. (2020). Shallow landslide susceptibility models based on  
 949 artificial neural networks considering the factor selection method and various non-linear  
 950 activation functions. *Remote Sensing*, 12(7), 1194. <https://doi.org/10.3390/rs12071194>.

951 Lee, J. U., Cho, Y. C., Kim, M., Jang, S. J., Lee, J., & Kim, S. (2022). The effects of different  
 952 geological conditions on landslide-triggering rainfall conditions in South Korea. *Water*,  
 953 14(13), 2051. <https://doi.org/10.3390/w14132051>.

954 Lee, M. J. (2016). Rainfall and landslide correlation analysis and prediction of future rainfall base  
 955 on climate change. In *Geohazards Caused by Human Activity*. IntechOpen.

956 Lee, S. G. (2009). *The Effects of Landslide in South Korea and Some Issues for Successful  
 957 Management and Mitigation*. 한국토양비료학회 학술발표회 초록집, 181-191.

958 Lee, S. W., Kim, G., Yune, C. Y., and Ryu, H. J. (2013). Development of landslide-risk assessment  
 959 model for mountainous regions in eastern Korea. *Disaster Advances*, 6(6), 70-79.

960 Li, B. V., Jenkins, C. N., & Xu, W. (2022a). Strategic protection of landslide vulnerable mountains  
 961 for biodiversity conservation under land cover and climate change impacts. *Proceedings  
 962 of the National Academy of Sciences*, 119(2), e2113416118.

963 Li, C. J., Guo, C. X., Yang, X. G., Li, H. B., & Zhou, J. W. (2022b, 2022). A GIS-based  
 964 probabilistic analysis model for rainfall-induced shallow landslides in mountainous  
 965 areas. *Environmental Earth Sciences*, 81(17), 432. [https://doi.org/10.1007/s12665-022-  
 10562-y](https://doi.org/10.1007/s12665-022-<br/>
  966 10562-y).

967 Liaw, A., and Wiener, M., (2002). Classification and regression by randomForest. *R News* 2(3),  
 968 18--22. Available at <https://journal.r-project.org/articles/RN-2002-022/RN-2002-022.pdf>  
 969 [Accessed 2025-01-24].

970 Liu, Y., Deng, Z., & Wang, X. (2024, 2021a). The effects of rainfall, soil type and slope on the  
 971 processes and mechanisms of rainfall-induced shallow landslides. *Applied Sciences*,  
 972 11(24), 11652. <https://doi.org/10.3390/app112411652>.

973 Liu, Z., Gilbert, G., Cepeda, J. M., Lysdahl, A. O. K., Piciullo, L., Hefre, H., and Lacasse, S.  
 974 (2021b). Modelling of shallow landslides with machine learning algorithms. *Geoscience  
 975 Frontiers*, 12(1), 385-393. <https://doi.org/10.1016/j.gsf.2020.04.014>

976 Luino, F., De Graff, J., Biddoccu, M., Faccini, F., Freppaz, M., Roccati, A., ... & Ungaro, F.,  
 977 D'Amico, M., and Turconi, L. (2022). The Role of soil type in triggering shallow  
 978 landslides in the alps (Lombardy, Northern Italy). *Land*, 11(8), 1125. <https://doi.org/10.3390/land11081125>.

979 Lusiana, N., Shinohara, Y., & Imaizumi, F. (2024). Quantifying effects of changes in forest age  
 980 distribution on the landslide frequency in Japan. *Natural Hazards*, 1-20.

981 Martinović, K., Gavin, K., Reale, C., and Mangan, C. (2018). Rainfall thresholds as a landslide  
 982 indicator for engineered slopes on the Irish Rail network. *Geomorphology*, 306, 40-50.  
 983 <https://doi.org/10.1016/j.geomorph.2018.01.006>

984 Mateos, R. M., López-Vinielles, J., Poyiadji, E., Tsagkas, D., Sheehy, M., Hadjicharalambous, K.,  
 985 ... & Herrera, G. (2020). Integration of landslide hazard into urban planning across  
 986 Europe. *Landscape and urban planning*, 196, 103740.

서식 지정함: 글꼴 색: 자동

서식 지정함: 글꼴 색: 자동

서식 지정함: 글꼴 색: 자동

서식 지정함: 글꼴 색: 자동

서식 지정함: 글꼴 색: 자동

서식 지정함: 글꼴 색: 자동

서식 있음: 탭: 4.5 글자(없음)

서식 지정함: 글꼴 색: 자동, 영어(미국)

서식 지정함: 글꼴 색: 자동

서식 지정함: 글꼴 색: 자동

서식 지정함: 글꼴 색: 자동

서식 지정함: 글꼴 색: 자동

서식 지정함: 글꼴 색: 자동

서식 지정함: 글꼴 색: 자동

서식 지정함: 글꼴 색: 자동

서식 지정함: 글꼴 색: 자동, 프랑스어(프랑스)

서식 지정함: 글꼴 색: 자동, 프랑스어(프랑스)

서식 지정함: 글꼴 색: 자동

서식 지정함: 글꼴 색: 자동

서식 지정함: 글꼴: +본문(Calibri), 11 pt, 글꼴 색: 자동, 영어(미국)

서식 있음: 탭: 4.5 글자, 왼쪽

서식 지정함: 글꼴 색: 자동, 프랑스어(프랑스)

서식 지정함: 글꼴 색: 자동

서식 지정함: 글꼴 색: 자동

서식 지정함: 글꼴 색: 자동

서식 있음: 탭: 4.5 글자, 왼쪽

서식 지정함: 글꼴 색: 자동

서식 지정함: 글꼴 색: 자동

988 McKenna, J. P., Santi, P. M., Amblard, X., and Negri, J. (2012). Effects of soil-engineering  
989 properties on the failure mode of shallow landslides. *Landslides*, 9, 215-228.  
990 <https://doi.org/10.1007/s10346-011-0295-3>.

991 McKight, P. E., and Najab, J. (2010). Kruskal-wallis test. *The corsini encyclopedia of psychology*,  
992 1-1. <https://doi.org/10.1002/9780470479216.corpsy0491>.

993 Meyer D, Dimitriadou E, Hornik K, Weingessel A, Leisch F (2021). *\_e1071: Misc Functions of  
994 the Department of Statistics, Probability Theory Group (Formerly: E1071), TU Wien\_*.  
995 R package version 1.7-9. ~~<https://CRAN.R-project.org/package=e1071>~~.  
996 <https://doi.org/10.32614/CRAN.package.e1071>.

997 Miao, F., Wu, Y., Xie, Y., and Li, Y. (2018). Prediction of landslide displacement with step-like  
998 behavior based on multialgorithm optimization and a support vector regression model.  
999 *Landslides*, 15, 475-488. <https://doi.org/10.1007/s10346-017-0883-y>.

1000 Montgomery, D. R., Schmidt, K. M., Dietrich, W. E., and McKean, J. (2009). Instrumental record  
1001 of debris flow initiation during natural rainfall: Implications for modeling slope stability.  
1002 *Journal of Geophysical Research: Earth Surface*, 114(F1).  
1003 <https://doi.org/10.1029/2008JF001078>

1004 Nguyen, Q. H., Ly, H. B., Ho, L. S., Al-Ansari, N., Le, H. V., Tran, V. Q., ... & Prakash, I., and  
1005 Pham, B. T. (2021). Influence of data splitting on performance of machine learning  
1006 models in prediction of shear strength of soil. *Mathematical Problems in Engineering*,  
1007 2021(1), 4832864. <https://doi.org/10.1155/2021/4832864>.

1008 O'brien, R. M. (2007). A caution regarding rules of thumb for variance inflation factors. *Quality  
1009 and quantity*, 41, 673-690. <https://doi.org/10.1007/s11135-006-9018-6>.

1010 Omwega, A. K. (1989). Crop cover, rainfall energy and soil erosion in Githunguri (Kiambu  
1011 District), Kenya. The University of Manchester (United Kingdom). Available at  
1012 <https://www.proquest.com/openview/dd7c169f804775d18041ec262d03e4c1/1?cbl=2026366&diss=y&pq-origsite=gscholar> [Accessed 2025-01-24].

1013 Panday, S., & Dong, J. J. (2021). Topographical features of rainfall-triggered landslides in Mon  
1014 State, Myanmar, August 2019: Spatial distribution heterogeneity and uncommon large  
1015 relative heights. *Landslides*, 18(12), 3875-3889. <https://doi.org/10.1007/s10346-021-01758-7>.

1016 Park, C. Y. (2015). The classification of extreme climate events in the Republic of Korea. *Journal  
1017 of the Korean Association of regional geographersRegional Geographers*,  
1018 21(2), 394-410. Available at  
1019 <https://koreascience.kr/article/JAKO201507740043627.page>. [Accessed: 2025-01-24]

1020 Park, S. J., & Lee, D. K. (2021). Predicting susceptibility to landslides under climate change  
1021 impacts in metropolitan areas of South Korea using machine learning. *Geomatics,  
1022 Natural Hazards and Risk*, 12(1), 2462-2476.  
1023 <https://doi.org/10.1080/19475705.2021.1963328>.

1024 Park, S.J. (2022). Assessment of disaster risks induced by climate change, using machine learning  
1025 techniques (Doctoral dissertation, 서울대학교 대학원).

서식 지정함: 글꼴 색: 자동

서식 지정함: 글꼴 색: 자동

서식 있음: 탭: 4.5 글자, 왼쪽

서식 지정함: 글꼴 색: 자동

서식 지정함: 글꼴 색: 자동

서식 지정함: 글꼴 색: 자동

서식 지정함: 글꼴 색: 자동, 영어(미국)

서식 지정함: 글꼴 색: 자동

서식 지정함: 글꼴 색: 자동

서식 지정함: 글꼴 색: 자동

서식 있음: 탭: 4.5 글자, 왼쪽

서식 지정함: 글꼴 색: 자동

서식 지정함: 글꼴 색: 자동

서식 지정함: 글꼴 색: 자동

서식 지정함: 글꼴 색: 자동

서식 지정함: 글꼴 색: 자동

서식 지정함: 글꼴 색: 자동

서식 지정함: 글꼴 색: 자동

서식 지정함: 글꼴 색: 자동

서식 지정함: 글꼴 색: 자동

서식 있음: 탭: 4.5 글자, 왼쪽

서식 지정함: 글꼴 색: 자동



1028 ~~Paudel, P. P., Omura, H., Kubota, T., and Morita, K. (2003). Landslide damage and disaster~~  
 1029 ~~management system in Nepal. *Disaster Prevention and Management: An International*~~  
 1030 ~~*Journal*, 12(5), 413-419.~~

1031 Pham, B. T., Tien Bui, D., and Prakash, I. (2018). Bagging based support vector machines for  
 1032 spatial prediction of landslides. *Environmental Earth Sciences*, 77, 1-17.  
 1033 <https://doi.org/10.1007/s12665-018-7268-y>

1034 Phillips, C., Hales, T., Smith, H., and Basher, L. (2021). Shallow landslides and vegetation at the  
 1035 catchment scale: A perspective. *Ecological Engineering*, 173, 106436.  
 1036 <https://doi.org/10.1016/j.ecoleng.2021.106436>

1037 Pisner, D. A., and Schnyer, D. M. (2020). Support vector machine. In *Machine learning* (pp. 101-  
 1038 121). Academic Press. <https://doi.org/10.1016/B978-0-12-815739-8.00006-7>

1039 ~~Pradhan, S., Toll, D. G., Rosser, N. J., & Brain, M. J. (2022). An investigation of the combined~~  
 1040 ~~effect of rainfall and road cut on landsliding. *Engineering Geology*, 307, 106787.~~  
 1041 ~~<https://doi.org/10.1016/j.enggeo.2022.106787>~~

1042 Pourghasemi, H. R., and Rahmati, O. (2018). Prediction of the landslide susceptibility: Which  
 1043 algorithm, which precision?. *Catena*, 162, 177-192. <https://doi.org/10.1016/j.catena.2017.11.022>

1045 Qiu, H., Regmi, A. D., Cui, P., Cao, M., Lee, J., and Zhu, X. (2016). Size distribution of loess  
 1046 slides in relation to local slope height within different slope morphologies. *Catena*, 145,  
 1047 155-163. <https://doi.org/10.1016/j.catena.2016.06.005>

1048 R Core Team (2022). R: A language and environment for statistical computing. R Foundation for  
 1049 Statistical Computing, Vienna, Austria. URL: ~~<<https://www.R-project.org/>>~~. Available at  
 1050 <https://www.R-project.org/> [Accessed 2025-01-24].

1051 Rahman, M. S., Ahmed, B., & Di, L. (2017). Landslide initiation and runoff susceptibility  
 1052 modeling in the context of hill cutting and rapid urbanization: a combined approach of  
 1053 weights of evidence and spatial multi-criteria. *Journal of Mountain Science*, 14(10),  
 1054 1919-1937. <https://doi.org/10.1007/s11629-016-4220-z>

1055 Ran, Q., Wang, J., Chen, X., Liu, L., Li, J., & Ye, S. (2022). The relative importance of  
 1056 antecedent soil moisture and precipitation in flood generation in the middle and lower  
 1057 Yangtze River basin. *Hydrology and Earth System Sciences*, 26(19), 4919-4931.  
 1058 <https://doi.org/10.5194/hess-26-4919-2022>

1059 Rathore, S. S., and Kumar, S. (2016). A decision tree regression-based approach for the number of  
 1060 software faults prediction. *ACM SIGSOFT Software Engineering Notes*, 41(1), 1-6.  
 1061 <https://doi.org/10.1145/2853073.2853083>

1062 Razakova, M., Kuzmin, A., Fedorov, I., Yergaliev, R., and Ainakulov, Z. (2020). Methods of  
 1063 calculating landslide volume using remote sensing data. In *E3S Web of Conferences* (Vol.  
 1064 149, p. 02009). EDP Sciences. <https://doi.org/10.1051/e3sconf/202014902009>

1065 Rosi, A., Peternel, T., Jemec-Auflič, M., Komac, M., Segoni, S., and Casagli, N. (2016). Rainfall  
 1066 thresholds for rainfall-induced landslides in Slovenia. *Landslides*, 13, 1571-1577.  
 1067 <https://doi.org/10.1007/s10346-016-0733-3>

서식 지정함: 글꼴 색: 자동

서식 있음: 탭: 4.5 글자, 왼쪽

서식 지정함: 글꼴 색: 자동

서식 지정함: 글꼴 색: 자동

서식 지정함: 글꼴 색: 자동

서식 지정함: 글꼴 색: 자동

서식 있음: 탭: 4.5 글자, 왼쪽

서식 지정함: 글꼴 색: 자동

서식 지정함: 글꼴 색: 자동

서식 지정함: 글꼴 색: 자동

서식 지정함: 글꼴 색: 자동

서식 지정함: 글꼴 색: 자동

서식 지정함: 글꼴 색: 자동

서식 있음: 탭: 4.5 글자, 왼쪽

서식 지정함: 글꼴 색: 자동

서식 지정함: 글꼴 색: 자동

서식 지정함: 글꼴 색: 자동

1068 Rotaru, A., Oajdea, D., and Răileanu, P. (2007). Analysis of the landslide movements. *International*  
1069 *journal of geology*, 1(3), 70-79. Available at [https://naun.org/multimedia/NAUN/](https://naun.org/multimedia/NAUN/geology/ijgeo-10.pdf)  
1070 [geology/ijgeo-10.pdf](https://naun.org/multimedia/NAUN/geology/ijgeo-10.pdf). [Accessed: 2025-01-24]

1071 Saito, H., Korup, O., Uchida, T., Hayashi, S., & Oguchi, T. (2014). Rainfall conditions, typhoon  
1072 frequency, and contemporary landslide erosion in Japan. *Geology*, 42(11), 999-1002.  
1073 <https://doi.org/10.1130/G35680.1>

1074 Saleh, A. M. E., Arashi, M., and Kibria, B. G. (2019). Theory of ridge regression estimation with  
1075 applications. John Wiley and Sons.

1076 Sato, T., Katsuki, Y., & Shuin, Y. (2023). Evaluation of influences of forest cover change on  
1077 landslides by comparing rainfall-induced landslides in Japanese artificial forests with  
1078 different ages. *Scientific reports*, 13(1), 14258. [https://doi.org/10.1038/s41598-023-](https://doi.org/10.1038/s41598-023-41539-x)  
1079 [41539-x](https://doi.org/10.1038/s41598-023-41539-x)

1080 Scheidl, C., Heiser, M., Kamper, S., Thaler, T., Klebinder, K., Nagl, F., Lechner, L., Markart, G.,  
1081 Rammer, W., and Seidl, R. (2020). The influence of climate change and canopy  
1082 disturbances on landslide susceptibility in headwater catchments. *Science of the total*  
1083 *environment* *Total Environment*, 742, 140588.  
1084 <https://doi.org/10.1016/j.scitotenv.2020.140588>

1085 Seger, C. (2018). An investigation of categorical variable encoding techniques in machine  
1086 learning: binary versus one-hot and feature hashing. Available at [https://www.diva-](https://www.diva-portal.org/smash/get/diva2:1259073/FULLTEXT01.pdf)  
1087 [portal.org/smash/get/diva2:1259073/FULLTEXT01.pdf](https://www.diva-portal.org/smash/get/diva2:1259073/FULLTEXT01.pdf). [last accessed: 2025-01-24]

1088 Shirzadi, A., Shahabi, H., Chapi, K., Bui, D. T., Pham, B. T., Shahedi, K., and Ahmad, B. B.  
1089 (2017). A comparative study between popular statistical and machine learning methods  
1090 for simulating volume of landslides. *Catena*, 157, 213-226. [https://doi.org/10.1016/](https://doi.org/10.1016/j.catena.2017.05.016)  
1091 [j.catena.2017.05.016](https://doi.org/10.1016/j.catena.2017.05.016)

1092 Singh, D., and Singh, B. (2022). Feature wise normalization: An effective way of normalizing data.  
1093 *Pattern Recognition*, 122, 108307. <https://doi.org/10.1016/j.patcog.2021.108307>

1094 Smith, H. G., Neverman, A. J., Betts, H., & Spiekermann, R. (2023). The influence of spatial  
1095 patterns in rainfall on shallow landslides. *Geomorphology*, 437, 108795.  
1096 <https://doi.org/10.1016/j.geomorph.2023.108795>

1097 Spiker, E. C., & Gori, P. (2003). *National landslide hazards mitigation strategy, a framework for*  
1098 *loss reduction (No. 1244)*. US Geological Survey.

1099 Stoof, C. R., Vervoort, R. W., Iwema, J., Van Den Elsen, E., Ferreira, A. J. D., & Ritsema, C.  
1100 J. (2012). Hydrological response of a small catchment burned by experimental fire.  
1101 *Hydrology and Earth System Sciences*, 16(2), 267-285. [https://doi.org/10.5194/hess-16-](https://doi.org/10.5194/hess-16-267-2012)  
1102 [267-2012](https://doi.org/10.5194/hess-16-267-2012)

1103 Sun, H. Y., Wong, L. N. Y., Shang, Y. Q., Shen, Y. J., and Lü, Q. (2010). Evaluation of drainage  
1104 tunnel effectiveness in landslide control. *Landslides*, 7, 445-454.  
1105 <https://doi.org/10.1007/s10346-010-0210-3>

1106 Székely, G. J., Rizzo, M. L., and Bakirov, N. K. (2007). Measuring and testing dependence by  
1107 correlation of distances. <https://doi.org/10.1214/009053607000000505>

서식 지정함: 글꼴 색: 자동

서식 지정함: 글꼴 색: 자동

서식 있음: 탭: 4.5 글자, 왼쪽

서식 지정함: 글꼴 색: 자동

서식 지정함: 글꼴 색: 자동

서식 지정함: 글꼴 색: 자동

서식 있음: 탭: 4.5 글자, 왼쪽

서식 지정함: 글꼴 색: 자동

서식 지정함: 글꼴 색: 자동

서식 지정함: 글꼴 색: 자동

서식 지정함: 글꼴 색: 자동

서식 지정함: 글꼴 색: 자동, 영어(미국)

서식 지정함: 글꼴 색: 자동, 영어(미국)

서식 지정함: 글꼴 색: 자동

서식 있음: 탭: 4.5 글자, 왼쪽

서식 지정함: 글꼴 색: 자동

서식 지정함: 글꼴 색: 자동

서식 지정함: 글꼴 색: 자동

서식 지정함: 글꼴 색: 자동

서식 지정함: 글꼴 색: 자동

서식 지정함: 글꼴 색: 자동

서식 있음: 탭: 4.5 글자, 왼쪽

서식 지정함: 글꼴 색: 자동

서식 지정함: 글꼴 색: 자동

1108 Tacconi Stefanelli, C., Casagli, N., & Catani, F. (2020). Landslide damming hazard  
 1109 susceptibility maps: a new GIS-based procedure for risk management. *Landslides*, 17,  
 1110 1635-1648. <https://doi.org/10.1007/s10346-020-01395-6>.

1111 Tsai, T. L., & Chen, H. F. (2010). Effects of degree of saturation on shallow landslides triggered  
 1112 by rainfall. *Environmental Earth Sciences*, 59, 1285-1295. <https://doi.org/10.1007/s12665-009-0116-3>.

1114 Turner, T. R., Duke, S. D., Fransen, B. R., Reiter, M. L., Kroll, A. J., Ward, J. W., Bach, J. L.,  
 1115 & Justice, T. E., and Bilby, R. E. (2010). Landslide densities associated with rainfall, stand  
 1116 age, and topography on forested landscapes, southwestern Washington, USA. *Forest  
 1117 Ecology and Management*, 259(12), 2233-2247. <https://doi.org/10.1016/j.foreco.2010.01.051>.

1119 Um, M. J., Yun, H., Cho, W., & Heo, J. H. (2010). Analysis of orographic precipitation on Jeju-  
 1120 Island using regional frequency analysis and regression. *Water resources  
 1121 managementResources Management*, 24, 1461-1487. <https://doi.org/10.1007/s11269-009-9509-z>.

1123 Van Tien, P., Luong, L. H., Due, D., Van Westen, C. J. (2000). The modelling of landslide hazards  
 1124 using GIS. *Surveys in geophysics*, 21(2), 241-255.  
 1125 <https://doi.org/10.1023/A:1006794127521>

1126 M., Trinh, P. T., Quynh, D. T., Lan, N. C., ... & Loi, D. H. (2021). Rainfall-induced catastrophic  
 1127 landslide in Quang Tri Province: the deadliest single landslide event in Vietnam in 2020.

1128 Wang, D., Hollaus, M., Schmaltz, E., Wieser, M., Reifeltshammer, D., & Pfeifer, N. (2016).  
 1129 Tree stem shapes derived from TLS data as an indicator for shallow landslides. *Procedia  
 1130 Earth and Planetary Science*, 16, 185-194. <https://doi.org/10.1016/j.proeps.2016.10.020>.

1131 Wei, Z. L., Shang, Y. Q., Sun, H. Y., Xu, H. D., and Wang, D. F. (2019). The effectiveness of a  
 1132 drainage tunnel in increasing the rainfall threshold of a deep-seated landslide. *Landslides*,  
 1133 16, 1731-1744. <https://doi.org/10.1007/s10346-019-01241-4>.

1134 Wiczorek, G. (1987). In central Santa Cruz Mountains, California. Debris flows/avalanches:  
 1135 process, recognition, and mitigation, 7, 93. Volume VII. *The Geological Society of  
 1136 America, Boulder, Colorado*.

1137 Willmott, C. J., & Matsuura, K. (2005). Advantages of the mean absolute error (MAE) over  
 1138 the root mean square error (RMSE) in assessing average model performance. *Climate  
 1139 researchResearch*, 30(1), 79-82. <https://doi.org/10.3354/cr030079>.

1140 Winter, M. G., & Bromhead, E. N. (2012). Landslide risk: some issues that determine societal  
 1141 acceptance. *Natural Hazards*, 62, 169-187.

1142 Yan, L., Xu, W., Wang, H., Wang, R., Meng, Q., Yu, J., and Xie, W. C. (2019). Drainage controls  
 1143 on the Donglingxing landslide (China) induced by rainfall and fluctuation in reservoir  
 1144 water levels. *Landslides*, 16, 1583-1593. <https://doi.org/10.1007/s10346-019-01202-x>.

1145 Yang, H., & Adler, R. F. (2008). Predicting global landslide spatiotemporal distribution: integrating  
 1146 landslide susceptibility zoning techniques and real time satellite rainfall estimates.  
 1147 *International Journal of Sediment Research*, 23(3), 249-257.

- 서식 지정함: 글꼴 색: 자동
- 서식 지정함: 글꼴 색: 자동
- 서식 지정함: 글꼴 색: 자동, 영어(미국)
- 서식 지정함: 글꼴 색: 자동, 영어(미국)
- 서식 지정함: 글꼴 색: 자동
- 서식 지정함: 글꼴 색: 자동
- 서식 지정함: 글꼴 색: 자동, 영어(미국)
- 서식 지정함: 글꼴 색: 자동
- 서식 지정함: 글꼴 색: 자동
- 서식 지정함: 글꼴 색: 자동
- 서식 지정함: 글꼴 색: 자동
- 서식 지정함: 글꼴 색: 자동
- 서식 지정함: 글꼴 색: 자동, 영어(미국)
- 서식 지정함: 글꼴 색: 자동, 영어(미국)
- 서식 지정함: 글꼴 색: 자동, 영어(미국)
- 서식 지정함: 글꼴 색: 자동
- 서식 있음: 탭: 4.5 글자, 왼쪽
- 서식 지정함: 글꼴 색: 자동
- 서식 지정함: 글꼴 색: 자동
- 서식 지정함: 글꼴 색: 자동
- 서식 있음: 탭: 4.5 글자, 왼쪽
- 서식 지정함: 글꼴 색: 자동
- 서식 지정함: 글꼴 색: 자동
- 서식 지정함: 글꼴 색: 자동
- 서식 있음: 탭: 4.5 글자, 왼쪽
- 서식 지정함: 글꼴 색: 자동



1148 Yoon, S. S., & Bae, D. H. (2013). Optimal rainfall estimation by considering elevation in the  
 1149 Han River Basin, South Korea. Journal of Applied Meteorology and Climatology, 52(4),  
 1150 802-818. <https://doi.org/10.1175/JAMC-D-11-0147.1>

1151 Yun, H. S., Um, M. J., Cho, W. C., & Heo, J. H. (2009). Orographic precipitation analysis with  
 1152 regional frequency analysis and multiple linear regression. Journal of Korea Water  
 1153 Resources Association, 42(6), 465-480. <https://doi.org/10.3741/JKWRA.2009.42.6.465>

1154 Yune, C. Y., Jun, K. J., Kim, K. S., Kim, G. H., and Lee, S. W. (2010). Analysis of slope hazard-  
 1155 triggering rainfall characteristics in Gangwon Province by database construction. Journal  
 1156 of the Korean Geotechnical Society, 26(10), 27-38. [https://doi.org/10.7843/kgs.  
 1157 2010.26.10.27](https://doi.org/10.7843/kgs.2010.26.10.27)

1158 Zachar, D. (2011). *Soil erosion*. Elsevier.

1159 Zaruba, Q., and Mencl, V. (2014). Landslides and their control. Elsevier. ISBN 0444600760,  
 1160 9780444600769

1161 Zhang, K., Wang, S., Bao, H., & Zhao, X. (2019). Characteristics and influencing factors of  
 1162 rainfall-induced landslide and debris flow hazards in Shaanxi Province, China. Natural  
 1163 Hazards and Earth System Sciences, 19(1), 93-105.  
 1164 <https://doi.org/10.5194/nhess-19-93-2019>

서식 지정함: 글꼴 색: 자동

서식 지정함: 글꼴 색: 자동

서식 지정함: 글꼴 색: 자동

서식 지정함: 글꼴 색: 자동

서식 지정함: 글꼴 색: 자동

서식 있음: 탭: 4.5 글자, 왼쪽

서식 지정함: 글꼴 색: 자동

서식 지정함: 글꼴 색: 자동

서식 지정함: 글꼴 색: 자동

서식 지정함: 글꼴 색: 자동

서식 지정함: 글꼴: 굵게 없음, 글꼴 색: 자동

서식 있음: 들여쓰기: 왼쪽: 0 cm, 내어쓰기: 9 글자, 줄  
 간격: 배수 1.15 줄, 단락의 첫 줄이나 마지막 줄 분리  
 방지, 금칙 처리 안 함, 단어 잘림 방지, 문장 부호 끌어  
 맞추지 않음, 탭: 4.5 글자, 왼쪽